AD 44483

QUARTERLY PROGRESS REPORT

RESEARCH ON PHYSICAL AND CHEMICAL PRINCIPLES AFFECTING HIGH TEMPERATURE MATERIALS FOR ROCKET NOZZLES

September 30, 1964

UNION CARBIDE RESEARCH INSTITUTE
Tarrytown, New York

Prepared by: Robert Lowrie
Robert Lowrie

Project Director: Verner Schomaker
Verner Schomaker

Project Supervisor: Richard W. Kebler
R. W. Kebler

Submitted by: S. R. Aspinall
S. R. Aspinall, Manager
UC Research Institute

Sponsored by
Advanced Research Projects Agency Propellant Chemistry Office,
ARPA Order No. 34-63, Task 4
Monitored by
Army Missile Command
Contract No. DA-30-069-ORD-2787
Project Code Number PRINCIPIA

FOREWORD

This research program is being carried out in the research laboratories of Union Carbide Corporation located at Tarrytown, New York (Union Carbide Research Institute). The work is supported by the Advanced Research Projects Agency Propellant Chemistry Office under Contract No. DA-30-069-ORD-2787 with the U. S. Army Missile Command, Redstone Arsenal, Alabama. The report period is from July 1, 1964 to September 30, 1964.

The program at Union Carbide Research Institute is supervised by Dr. Richard Kebler under the project direction of Dr. Verner Schomaker with Dr. S. R. Aspinall serving as general project coordinator and Manager of the Institute.

The scope of the program as stated in the contract is "to obtain a better understanding of the mechanisms which govern the behavior of materials in high-temperature environments, to learn how to make the most effective use of available materials, and to obtain a better knowledge of optimum properties desired for new materials for particular use. The work is expected to provide guidance for those concerned with the development of materials and the use of materials in solid-propellant engines."

TABLE OF CONTENTS

I SUMMARY

Data have been obtained on the corrosion of W by CO_2/Ar mixtures with CO_2 stagnation partial pressures of 40, 81, 122, 192, and 340 torr at 2325-3000°K and 340-torr total stagnation pressure. The reaction rate is linear with time. At the lower temperatures log rate is nearly linear with reciprocal temperature for all CO_2 partial pressures, and near 3000°K the rates approach those calculated for diffusion control. These data on the CO_2-W reaction have been analyzed in terms of an approximate forward rate expression for the surface-controlled region, a mass-transfer treatment, and an assumed reverse reaction. The calculated curves agree well with the experimental data, although some questions remain to be resolved; measurements have been made of the corrosion rates of tungsten in mixtures of CO_2, CO, and Ar to help clarify these points.

Design improvements have been made in the high-pressure stagnation-flow reactor, and the corrosion of tungsten by CO_2 at a stagnation pressure of 1033 torr from 2080 to 2850°K has been measured. A linear plot of log of corrosion rate vs. 1/T was obtained up to about 2650°K with an apparent activation energy comparable to that obtained in the low-pressure reactor. Some difficulty has been encountered in controlling temperatures in this reactor. Study of the CO_2-W reaction in the arc-image reactor has been extended to a gas velocity of 9000 cm/sec, and the results obtained are consistent with previous data. Appreciable differences have been found in the rates and modes of attack of CO_2 on tungsten specimens differing in density and in orientation relative to the direction of working.

The potential flow calculation for gas flow in the exterior region for stagnation geometry has been extended by the inclusion of a second-order perturbation calculation of compressibility effects.

A kinetic model has been deduced which fits the experimental mass-spectrometric data obtained on the reaction of oxygen at low pressures with tungsten over the temperature range 1400-3150°K. The model involves two adsorption sites for oxygen: essentially, bare tungsten and tungsten with a monolayer of oxygen. Experiments using atomic oxygen generated at one W filament to strike a second tungsten filament appear to confirm the high

sticking probability for oxygen molecules assumed for the second type of adsorption site. Preliminary studies of the Nb-O_2, Ta-O_2, W-CO, W-CO_2, and Mo-O_2 systems by mass spectroscopy have begun.

High-density tungsten rod of 1-1/2 inch diameter has been obtained to make nozzles whose corrosion will be tested in a new high-pressure liquid motor by the Army Missile Command. An initial calculation was made of the temperature history to be expected for such a nozzle.

The accuracy of our least-squares program for computing lattice parameters was checked by determining the lattice parameter of a tungsten sample from measurements of the positions of the peaks and of the centers of gravity of the lines with the Siemens diffractometer. The lattice parameter computed from the peak-position measurements agrees very closely with the average of values obtained by ten other laboratories on presumably identical samples; the center-of-gravity measurements led to a value low by a small amount. These results establish the overall accuracy of our techniques and apparatus. In the study of the thermal expansion of NbB_2 and TaB_2 by measurements of lattice parameter vs. temperature, surface depletion in boron was found for samples heated above 1200°C in a vacuum. Since the lattice parameters of these borides are also dependent on boron content, such losses must be prevented before meaningful measurements can be made above 1200°C. New data have been obtained for TiB_2 up to 1250°C. These agree well with previous measurements and show no evidence for boron depletion.

All the first-order elastic constants of polycrystalline tungsten have been computed for temperatures from 24° to 1800°C from measurements of the velocities of shear and compressional waves. The data are in good agreement with published data extending to 760° and 1200°C. Difficulties in bonding tungsten crystals to buffer rods have been overcome, and data to complete our set of single-crystal elastic constants of tungsten to 1800°C will be obtained.

Several creep tests were made on polycrystalline TiC, and a large stress dependency ($\varepsilon \cong P^{10}$) was found for creep at 2243°K. Appreciable quantities of zirconium and vanadium were found to have been present in TiC specimens that showed low creep rates, and these impurities might well explain

the strengthening. The new electron-beam zone-refining equipment has produced refined tungsten rods, but of somewhat irregular shape. A power supply to control the heating current is being considered to overcome this problem. The vacuum tensile tester is being checked, and methods for electrolytic machining of specimens developed. A discussion of Li's theory of creep as applied to tungsten single crystals is given.

A pyrohydrolysis technique for the determination of boron has been successfully developed for TiB_2 and ZrB_2. This procedure considerably simplifies the analysis and appears to increase its precision. Preliminary experiments have been conducted on the analysis of other borides by this method.

Materials preparation work has been concentrated on the preparation of composite materials consisting of interpenetrating skeletons of refractory compounds and metals. Porous bodies of the refractory compounds were fabricated by hot pressing and infiltrated with metals by an improved technique. Isostatic pressing is being investigated as an alternative method which would permit forming larger porous bodies for infiltration than will hot pressing. The impact strengths of porous and of nickel-infiltrated TaC were measured. Infiltration considerably increases the impact strength of TaC and renders it comparable to the strengths of conventional cemented carbides. The transverse rupture strength of hot-pressed TaC goes through a minimum at 1400°C and then increases considerably. This is probably associated with the beginning of plastic deformation. Nickel-infiltrated TaC rapidly decreases in strength above 1000°C and has little or no strength at 1400°C. This is probably a result of the dissolution of TaC-TaC grain boundaries by the nickel near 1400°C.

II INTRODUCTION

This program is concerned with the principles governing high-temperature chemical and physical behavior, especially in the respects that may contribute importantly to the successful performance of materials as rocket components operating at high temperatures.

The materials being studied here are tungsten, graphite, and the refractory carbides and borides of the transition metals. These carbides and borides are difficult to handle because of their high melting points, brittleness and high hardness at room temperature, and susceptibility to contamination at high temperatures. Thus, a considerable effort is devoted to their purification and fabrication. Composite bodies consisting of interpenetrating carbide and metal skeletons are being prepared and evaluated. These appear to hold promise for high-temperature service, especially in rocket nozzles.

Because corrosion of rocket nozzles by the exhaust gases is a serious problem, reaction rates between various gases or combinations of gases and possible nozzle materials are being studied as functions of temperature and pressure in this program. However, at typical temperatures for rocket operation these gas-solid reactions may be controlled not by the surface reaction rate but partly or entirely by the rates of diffusion of reactants to the surface or of products away from it. Special efforts are being made to measure truly surface-controlled reaction rates for the various refractory materials at all temperatures of interest by using experimental conditions that afford very high mass-transfer rates. The values so obtained will permit calculation of corrosion rates for conditions where both surface reaction rate and diffusion are important.

As structural parts, rocket nozzles are subjected to substantial stresses during operation. Some of these stresses change relatively slowly with time, and their effects on the nozzle will be determined by creep strength and ductility. There are also rapidly changing stresses, resulting from sudden heating or cooling, which can cause deformation or fracture. The thermal stress developed by a given temperature change increases with increasing coefficient of expansion or elastic modulus, and decreases with increasing thermal conductivity or specific heat, and the likelihood of fracture due to these stresses further depends upon the tensile strength and ductility. Measurements are being made of several of these important properties.

III. TECHNICAL RESULTS AND PLANS

A. Gas-Solid Reactions

Introduction

In the September, 1963 Quarterly Progress Report (QPR) we discussed in some detail the relationship between gas-phase diffusion and the measurements of the kinetics of gas-solid reactions. In both that report and the following one (QPR, December 1963), it was pointed out that many important corrosive reactions will be diffusion-controlled at high temperatures under the conditions of particular applications, while under other conditions the surface kinetics may determine the extent of corrosion. It is essential, therefore, if the effect of a corrosive environment on a refractory material is to be predicted, that rate expressions for the potential reactions be available from laboratory studies approaching as closely as possible the conditions of temperature and pressure of that environment. However, because slowness of gas-phase diffusion can interfere with the laboratory measurements just as it affects the practical situations, it is essential that apparatus be designed to minimize the hindrance of diffusion; to do this it is clearly necessary that the diffusion-limited case be understood for each experimental arrangement designed to obtain kinetic data at high temperatures.

Our objectives in this program are, first, the determination of the surface-controlled rates of reactions between gaseous rocket exhaust components and actual or potential rocket nozzle materials in the range of temperatures and pressures characteristic of rocket operations, and, second, the development of methods of applying such rate data, in conjunction with aerodynamic analyses, to predict corrosion rates in the transition region between surface and diffusion control. To weigh the extent of control by gaseous diffusion we have analyzed and are continuing to analyze all the data obtained in this program to determine where diffusional effects are important.

We have designed and built a number of experimental reactors in which high mass-transfer rates are achieved through use of high velocity gas streams impinging in stagnation patterns on hot samples; the effect of this is,

for a given reaction, to raise very considerably the temperatures at which gaseous diffusion becomes important in determining observed reaction rates, thus allowing the measurement of purely surface-controlled reaction rates to be made at higher temperatures than otherwise possible. Section A-4 continues the development of the theory of mass transfer in such systems.

Further results of the study of the oxidation of tungsten by CO_2 in our sub-atmospheric stagnation-flow reactor are presented in Section A-1, along with a preliminary analysis of the kinetics and of the effect of gaseous diffusion. The material in this section was the basis for a paper presented September 3 at the Symposium on High-Temperature Inorganic Chemistry sponsored by the Inorganic Chemistry Division of the Chemical Institute of Canada, in Ottawa. The first results obtained in our higher pressure reactor, also on the CO_2-W reaction, are described in Section A-2, and an investigation of the effect of tungsten structure on this reaction in Section A-3.

The experimental arrangements described above, though capable of yielding rate expressions at temperatures and pressures of direct interest in rocket propulsion, all operate under conditions that preclude observation of the details of the gas-surface reaction mechanisms. To obtain this type of information mass-spectrometric studies of reactions at very low pressures are being conducted; further details of the investigation of the O_2-W reaction and initial results on some other systems are given in Section A-5.

1. Kinetics of the Oxidation of W by CO_2 J.M. Quets, R.A. Graff, P.N. Walsh

The induction-heated stagnation-flow reactor being used to measure rates of corrosion of tungsten by carbon dioxide at pressures below one atmosphere has been described previously (March, 1964 QPR and June, 1964 QPR). Briefly, the experiments involve flowing a metered mixture of Ar and CO_2 at room temperature in a stream perpendicular to one face of a cylindrical tungsten sample heated by a current concentrator. The total pressure of the reacting mixture is the stagnation pressure over the tungsten surface and the temperature of the reacting surface is measured by an optical pyrometer during the course of the experiment. The rate of surface recession at the stagnation point is the desired reaction rate; it is ordinarily multiplied by the ratio of the density of tungsten to its atomic weight to obtain the rate in moles cm^{-2} $sec.^{-1}$.

It was demonstrated in Section A-3 of the June, 1964 QPR that under some of our experimental conditions the surface rate effectively determines the observed reaction rate while under other conditions gaseous diffusion severly limits the rates attainable. It was reported in Section A-4 of the June 1964 QPR and is demonstrated in more detail in Section A-3 of this report that the reacted samples show different degrees of gross surface roughness as the result of reaction, this roughness being greater when the reaction occurs under conditions approximating surface rate control than when gaseous diffusion is important. Such differences in sample surface condition presumably cause differences in emittance of the various samples and hence in the correction required to convert brightness temperature to true temperature. We have initiated, but not completed, spectral reflectance measurements on the samples to determine the emittances. Therefore, all temperatures in this section, which are based on an assumed invariant emittance, are to be considered as provisional.

During this quarter, data on the corrosion of tungsten with Ar/CO_2 mixtures were obtained for CO_2 stagnation partial pressures of 40, 81, 122, 192, and 340 torr over the temperature range 2325-3000°K. The partial pressure of carbon dioxide was varied by varying the relative flows of CO_2 and Ar, keeping the total flow (Ar + CO_2) from the 1/4" diameter nozzle at 84 standard

liters/minute (SLM). The total static pressure in the reactor was 300 torr and the measured total stagnation pressure was 340 torr.

The stagnation point recession at CO_2 partial pressures of 40 and 81 torr was reported (June, 1964 QPR) to be linear with time. The same behavior was observed at CO_2 partial pressures of 122 and 340 torr (Figure A-1). The rates of corrosion at the five different CO_2 partial pressures (Figure A-2) all show the same type of temperature dependence: At the lower temperatures, the plot of log rate vs. reciprocal temperature is linear, corresponding essentially to surface-control, but at the higher temperatures gaseous diffusion starts to compete with the surface reaction for the slow step of the overall reaction. This effect is shown on the isobar by a decreasing apparent activation energy as the temperature increases. At the highest temperatures the rates at each CO_2 partial pressure approach those calculated (cf June, 1964 QPR) for complete diffusion control (not shown in the figure).

Since in many practical situations as well as in our experiments it is necessary to contend with diffusional interference, it is important that efforts be made to analyze the behavior of reactions in the transition region between surface rate control and diffusion control so as to separate the two effects. An obvious advantage to be gained is the extension of the temperature range for which the true surface rate may be represented by a formal rate equation; in addition, one gains the power to predict rates in the transition region wherever the diffusion limit can be estimated. As a first step toward these goals we have analyzed the data on the CO_2-W reaction obtained to date. The first step in this analysis is the derivation of an approximate forward rate expression for the surface controlled region; next this is combined with a mass transfer treatment and some simple assumptions about the reverse reaction and attempts made to predict the transition region. Ultimately, we hope to be able to use the transition region data alone to derive the surface rate expression.

To obtain a trial surface rate expression we treat the data on the assumption that diffusional effects are negligible, i.e. that the effective CO_2 pressure is the free stream value. This assumption ought to be quite good at the lowest temperatures and get progressively worse at higher where diffusion affects the rates more. Employing this approximation, plots of the dependence

of corrosion rate on CO_2 partial pressure at several temperatures (Figure A-3) were derived from the temperature-dependence curves, Figure A-2. The shapes of these rates vs P_{CO_2} curves suggest that the following empirical equation (sometimes referred to as a Langmuir-type rate equation) may be an appropriate representation of these results.

$$\text{Rate} = \frac{a\ P_{CO_2}}{1 + b\ P_{CO_2}} \tag{1}$$

The constants a and b are assumed to be temperature dependent:

$$a = Ae^{-\alpha/RT} \tag{2}$$

$$b = Be^{-\beta/RT} \tag{3}$$

At a given temperature a and b may be obtained from equation 1 by taking the reciprocals of both sides:

$$\frac{1}{\text{Rate}} = \frac{1}{a\ P_{CO_2}} + \frac{b}{a} \tag{4}$$

and plotting reciprocal rate vs $1/P_{CO_2}$; the slope is then 1/a and the intercept b/a. Replotting the data of Figure A-3 in this way (Figures A-4 and A-5) yields values of a and b that have the temperature dependence required by equations 2 and 3 (Figure A-6* and A-7) up to approximately 2600°K. From the slopes and intercepts of Figures A-6 and A-7 we obtain A = 13,000 moles cm^{-2} sec^{-1} atm^{-1}, B = 92.4 atm^{-1}, α = 90 kcal/$mole^{-1}$ and β= 23 kcal/$mole^{-1}$. The value of α is, as expected, slightly greater than the apparent activation energy that would be derived from the linear portions of Figure A-2; the value of β however, is surprising, being of the opposite sign to what would be predicted by any of a variety of mechanisms that might lead to a rate expression of the form of Equation 1.

At the stage at which it was necessary to choose a form of forward rate expression to use in the combined kinetics--mass-transfer treatment

---

* Above 2575°K, values of a were not obtained from the 1/rate vs $1/P_{CO_2}$ plots because these were not clearly linear; instead, the initial slopes of the rate vs P_{CO_2} curves (Figure A-3) were used for a above this temperature.

described below, it was recognized that this discrepancy was most probably due to back reaction (owing to products piling up at the surface because they cannot diffuse away as rapidly as formed) being hidden in the term $B\,P_{CO_2}e^{-\beta/RT}$; whether such a term was genuinely important was questionable. Nevertheless, it was included.

This being our first attempt at a combined kinetics--mass-transfer calculation, we have written a computer program specific for the CO_2-W system, leaving for later the type of general approach that was used in the consideration of diffusion-controlled reactions alone (March, June, 1964 QPR). A major simplification has been introduced from the start: since there is only one experimentally measured quantity, the rate of loss of tungsten, we have considered this loss to occur through one reaction only, viz.

$$CO_2(g) + \tfrac{1}{3}\,W \longrightarrow 1/9\;W_3O_9(g) + CO(g). \qquad (5)$$

This reaction was chosen because our previous calculations for the diffusion limit (March, 1964 QPR) indicated that W_3O_9 was the principal tungsten-containing species expected in the temperature range of our experiments when the reaction is diffusion controlled. The measurements at 40 torr CO_2 and 8.06 SLM total flow reported in the June, 1964 QPR indicated that the rate vs temperature curve goes over smoothly from the apparently surface-rate controlled to the apparently diffusion-controlled condition; hence we have assumed, for the present at least, that reaction 5 is the principal reaction to be considered under all conditions encountered in this study.

In the combined diffusion-kinetic treatment we first write the rate equation in the form

$$r = \frac{A\,P_{CO_2}e^{-\alpha/RT}}{1 + B\,P_{CO_2}e^{-\beta/RT}}\left(1 - \frac{P_{CO}\,P_{W_3O_9}^{1/9}}{K\,P_{CO_2}}\right) \qquad (6)$$

where r is the molar rate of loss of tungsten, the P's are partial pressures at the reaction interface, and K is the equilibrium constant for reaction 5. The first term on the right is the forward rate expression and the second a simple back-reaction expression where the reverse rate of reaction 5 is assumed to be proportional to the partial pressures of the products raised to powers

equal to the coefficients in reaction 5. The back reaction term was chosen to cause the rate to go to zero when the gas composition at the reaction interface satisfies the equilibrium constant for reaction 5.

For each of the gaseous species in reaction 5 we write a diffusion equation

$$\nu_j r = k_j (P'_j - P_j) \tag{7}$$

where r and P_j have the same significance as in equation 6, ν_j is the stoichiometric coefficient of the jth species in reaction 5, P'_j is the free stream partial pressure of the jth species, and k_j its transport coefficient given by (cf September, December, 1963 QPR)

$$k_j = \frac{C\, D_{jm} Nu}{P_{fj} d} \tag{8}$$

where c is the gas concentration, d the characteristic dimension of the system, D_{jm} the mean diffusion coefficient and P_{fj} the "film pressure factor" for component j, and Nu the Nusselt number for mass transfer in the system. Solution of equations 6 and 7 for r should yield the corrosion rate over the whole temperature range, including the reaction-controlled, transition, and diffusion-controlled regions.

Trial runs were made with this scheme using the constants A, B, α, and β derived as described above from the data below 2575°K. The shape of the isobars (Figure A-2) reproduced very well though the calculated rates were always lower than the observed; this discrepancy appeared to be due to the neglect of the back reaction term in the earlier treatment having attributed undue importance to the term $BP_{CO_2} e^{-3/RT}$. The qualitative fit encouraged us to attempt to derive values of the constants in the rate equation by fitting the data to equations 6 and 7 by a least squares method, a non-linear least squares program applicable to this type of problem being available in the Computer Center library. In undertaking this it was thought advisable to recognize the uncertainty in the estimated diffusion limit, i.e. in Nu. The correlation we have been using for mass transfer in this reactor[1] gives

$$Nu = 0.167\ Re^{0.64} Sc^{1/3} \tag{9}$$

---

(1) V. A. Smirnov, G. E. Verevochkin, and P. M. Brdlick, Int. J. Heat and Mass Transfer 2, 1 (1961).

where Re and Sc are the Reynolds and Schmidt numbers for the flowing gas. Within the range of variation in gas-flow conditions employed here this may be approximated by

$$Nu = Nu' \ (F/F')^{2/3} \qquad (10)$$

where Nu' is a "reference" Nusselt number evaluated for a "reference" mass flow rate F' and F is the mass flow rate for a particular experiment. An approximate value of Nu' was computed from the properties of argon gas and Nu' was made a parameter to be fitted in the least squares calculation along with A, B, α, and β from the rate equation.

Testing of the least squares curve fitting program has been carried forward using the provisional temperatures in order to investigate the efficiency of the program and determine what quality of fit is to be expected. The results obtained after 40 iterations, in which a true minimum in the sum of the squares of the rate residuals was not obtained, are shown in Figures A-8 to A-10. The model chosen provides a reasonable description of the behavior of the system, at least at the higher CO_2 pressures and flow rates. The number of cycles of adjustment required indicates, however, that the fitting routine is not very efficient. This difficulty arises from the insensitivity of the calculated rates (and therefore the sum of squares of residuals) to the term $B\ P_{CO_2} e^{-\beta/RT}$ which appears in the denominator. Relatively large changes in the strongly-coupled parameters B and β, if in the opposite sense, affect the residuals very little; the program has apparently been wasting a lot of time in trials of this type of adjustment. While the constants B and β are very poorly defined, so that it is premature to draw conclusions, it is interesting that the computer achieves its best fit (to date) by making β negative; this, and the observation that the term $B\ P_{CO_2} e^{-\beta/RT}$ is about 5-6% of the denominator for the highest CO_2 pressures employed suggests that the term may have a real significance. Higher pressure CO_2 data are desireable to help decide this point — initial results obtained in our high pressure stagnation-flow reactor are described in section A-2.

The data obtained at 40 torr CO_2 at a total flow rate of 8 SLM are seen (Figure A-10) to be least well fitted by the model chosen; though the absolute deviations between observed and calculated rates are approximately the same magnitude for this isobar as for all the others, in this case the

deviations are systematic. It is possible that this is a result of the emittance uncertainty; if, as hypothesized, the samples reacted under conditions more nearly reaction-controlled have higher emittances than those more nearly diffusion controlled, then most of the 84 SLM curve and the lower temperature region of the 8 SLM curve in Figure A-10 would be shifted to lower temperatures and a better qualitative agreement between observed and calculated temperature dependences obtained. Alternatively, it is possible that the backward reaction rate expression chosen for consideration is not the best choice. The 8 SLM curve, which most closely approaches the diffusion limit, is most sensitive to the back reaction term in the rate equation. Further information pertinent to the question of the proper back-reaction expression is being sought through study of the corrosion by mixtures of CO_2 and CO.

The rates of corrosion at different CO/CO_2 ratios in the reacting gas, obtained by mixing varying flows of CO_2 and CO with a fixed flow of Ar, are compared in Figure A-11. The lines through each data set were drawn parallel to the $CO/CO_2 = 0$ isobar line. For the data obtained thus far, the flow of Ar was kept constant at 54 SLM and the total flows of CO_2 + CO at 30 SLM. The static pressure in the reactor was 300 torr. These conditions were chosen for ease of comparing the Ar-CO_2-CO data with the previous Ar-CO_2 data. For a $CO/CO_2 = 0$ ratio, the CO_2 stagnation partial pressure was 122 torr. Detailed analysis of these results is under way.

Future Work

The amount and type of further experimental work to be done on the CO_2-W reaction will be decided on the basis of the analysis, which is continuing. At present it appears that higher pressure data are most needed, so emphasis will be given to this phase of the work.

Modification of the sub-atmospheric pressure reactor for the study of the tungsten/water vapor reaction has begun. The water vapor will be supplied by a 6 KW electric boiler capable of delivering 20 lbs. of vapor per hour at a maximum pressure of 100 PSIG. The boiler will be fed with distilled water. The water vapor will be metered by a critical flow nozzle and mixed with a preheated flow of Ar. All connections to the reactor and the nozzle will be heated to a constant temperature to avoid any condensation of water vapor.

This investigation will be started as soon as the equipment has been assembled.

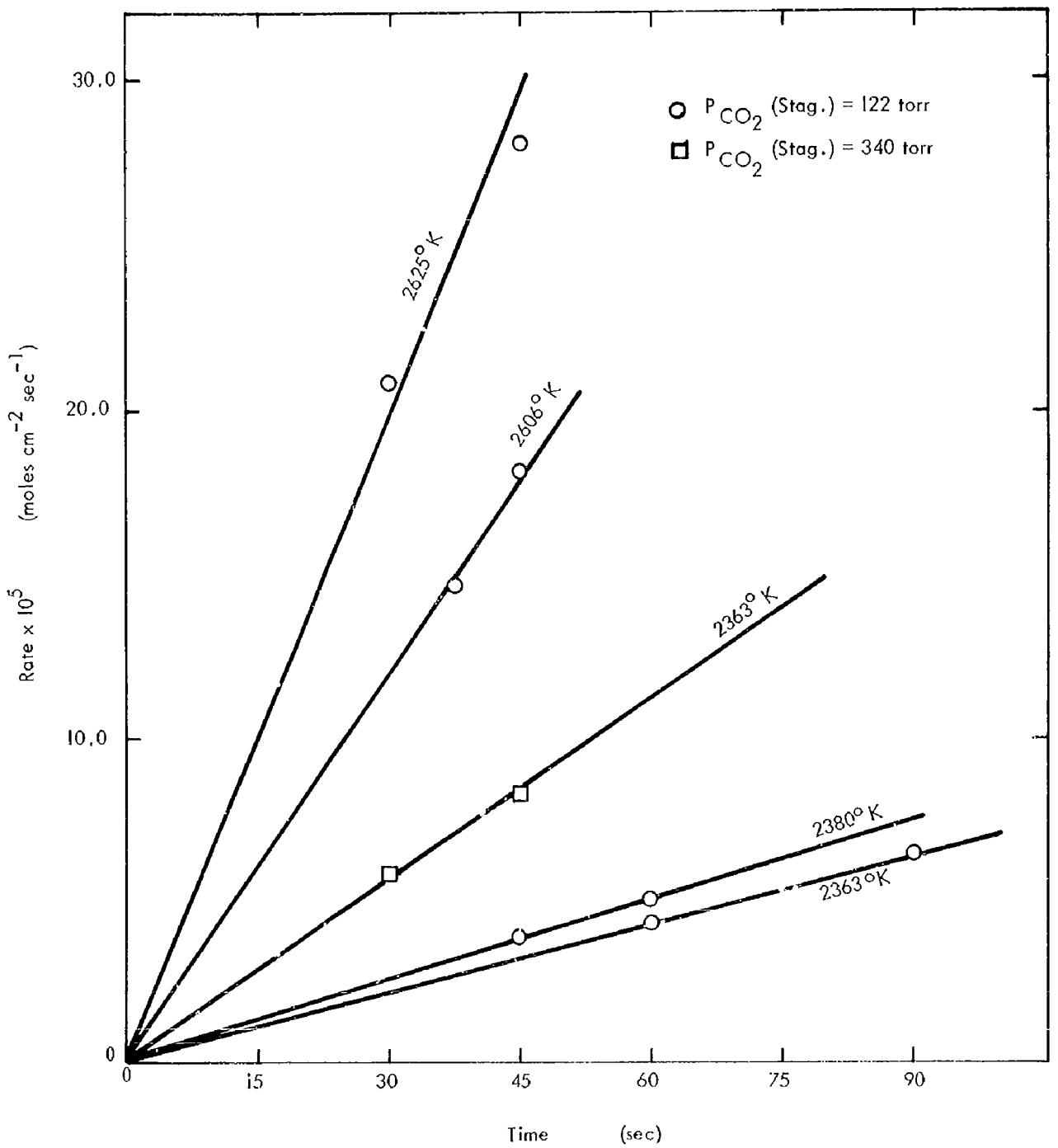

FIGURE A - 1 TIME DEPENDENCE OF THE RATE OF CORROSION OF TUNGSTEN BY CO_2

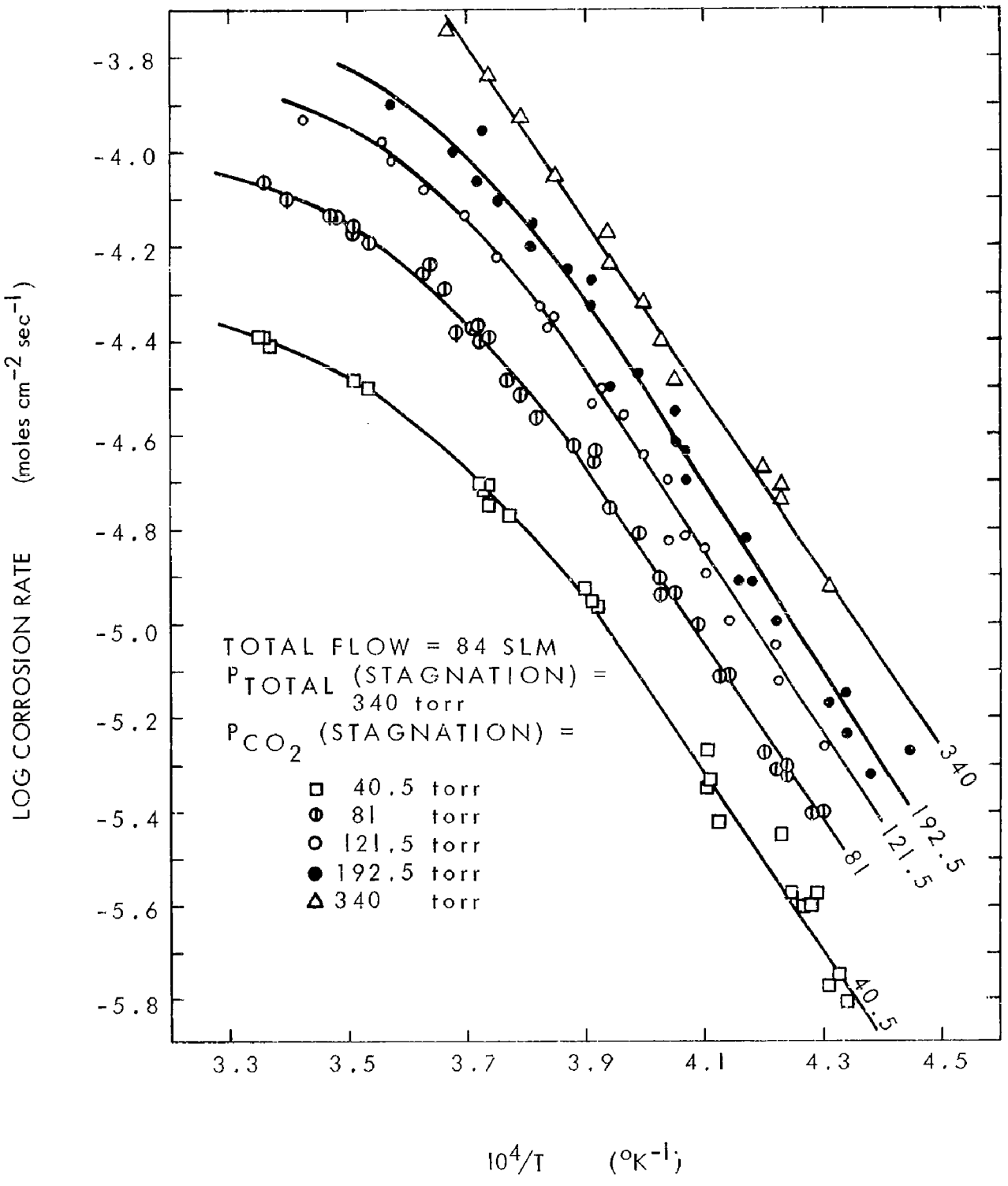

FIGURE A - 2 TEMPERATURE DEPENDENCE OF CORROSION OF W BY CO_2 AT SEVERAL CO_2 PRESSURES

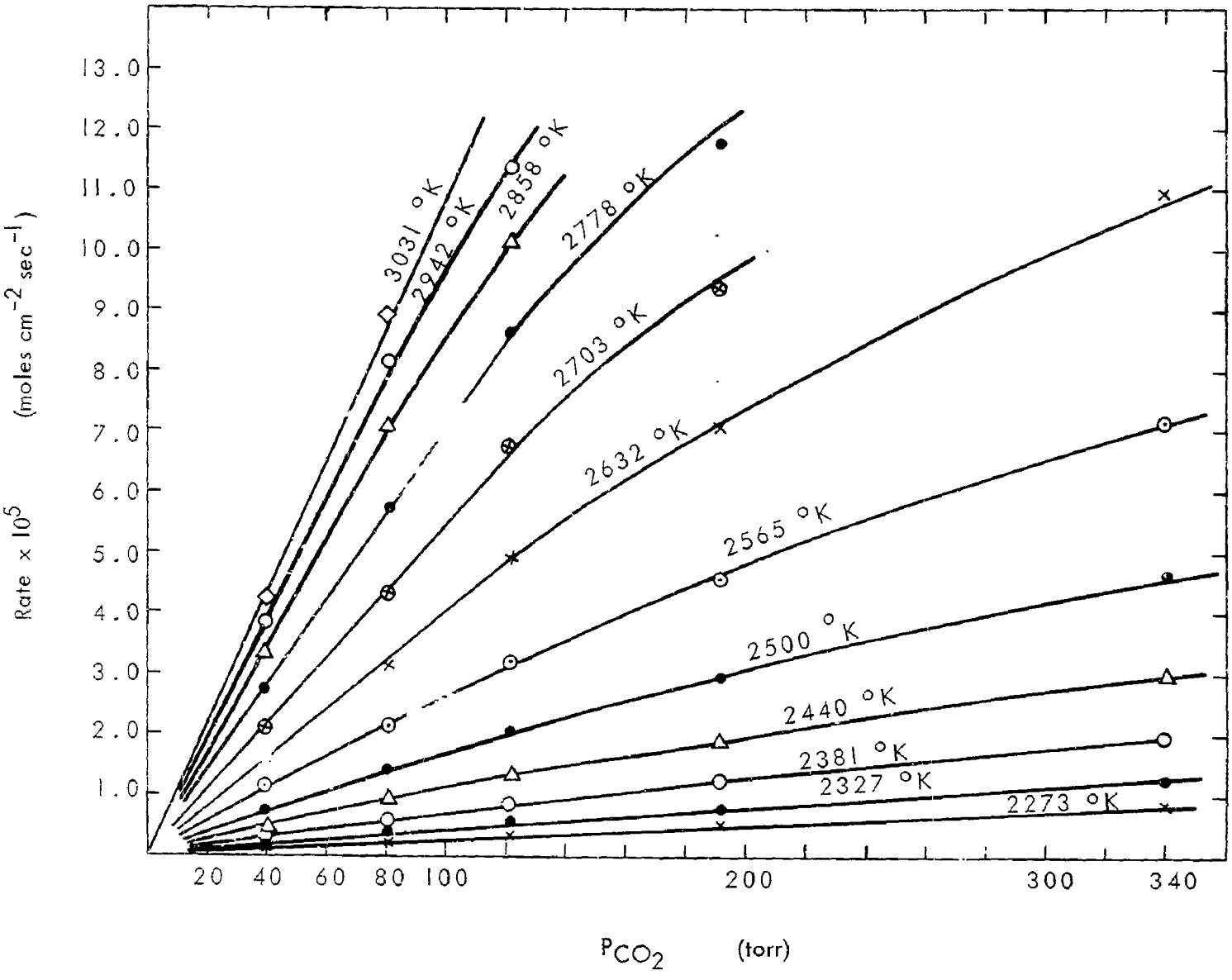

FIGURE A - 3 PRESSURE DEPENDENCE OF CORROSION OF W BY CO_2 AT CHOSEN TEMPERATURES

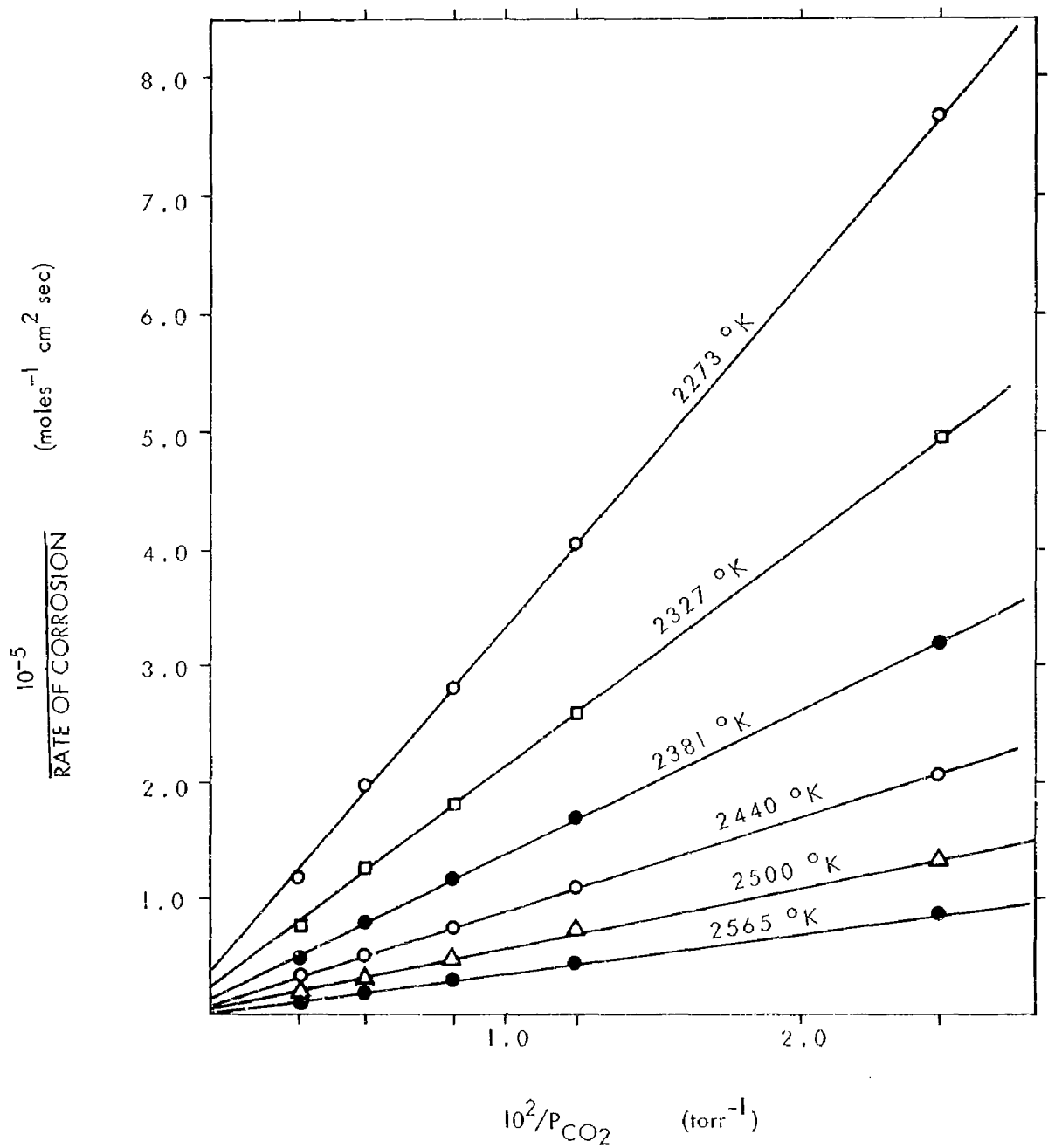

FIGURE A - 4 RECIPROCAL RATE VS. RECIPROCAL CO_2 PRESSURE AT 2273 TO 2565°K

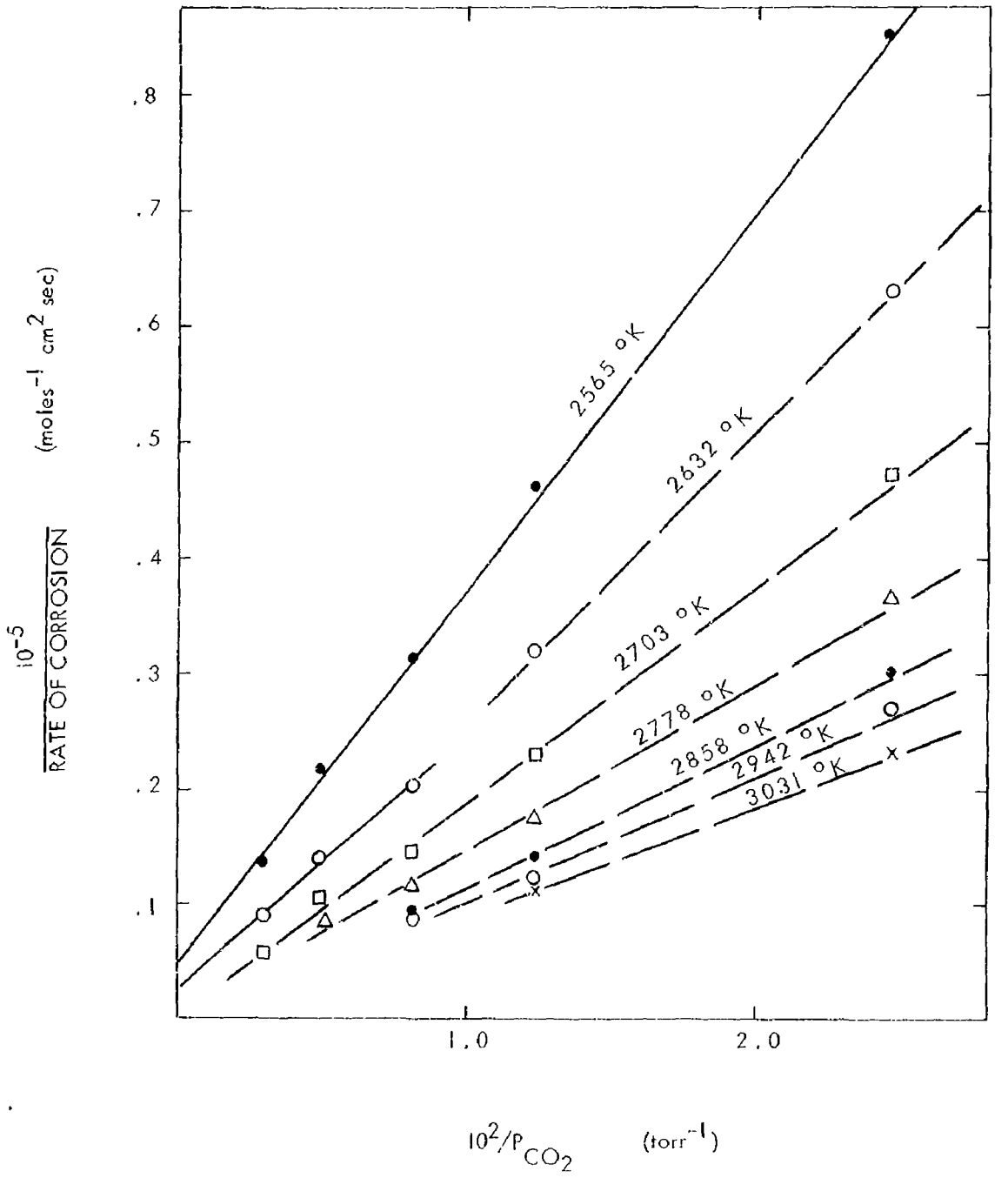

FIGURE A - 5 RECIPROCAL RATE VS. RECIPROCAL CO_2 PRESSURE AT 2565 TO 3031°K

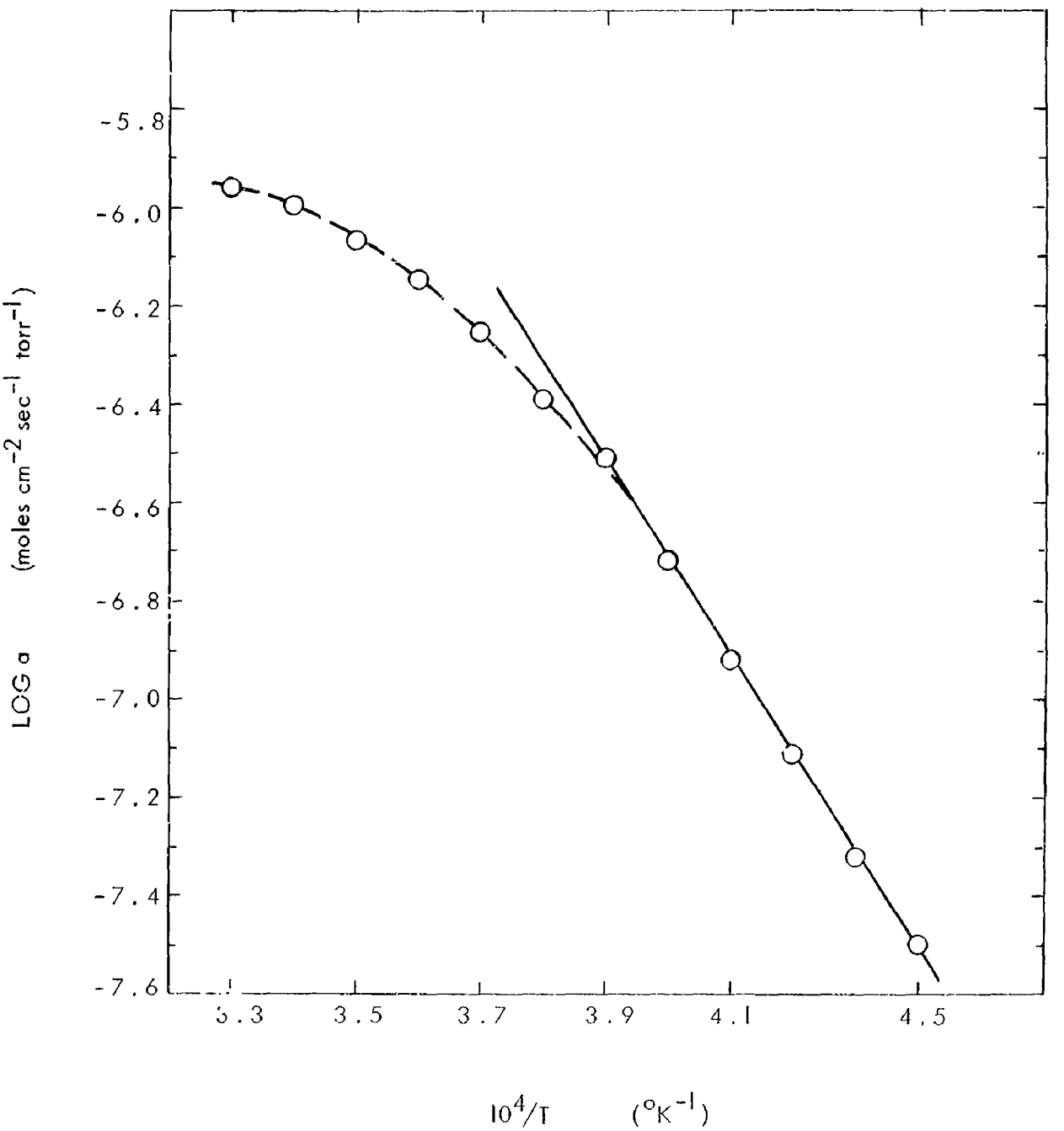

FIGURE A - 5 TEMPERATURE DEPENDENCE OF PARAMETER $\underline{a}$

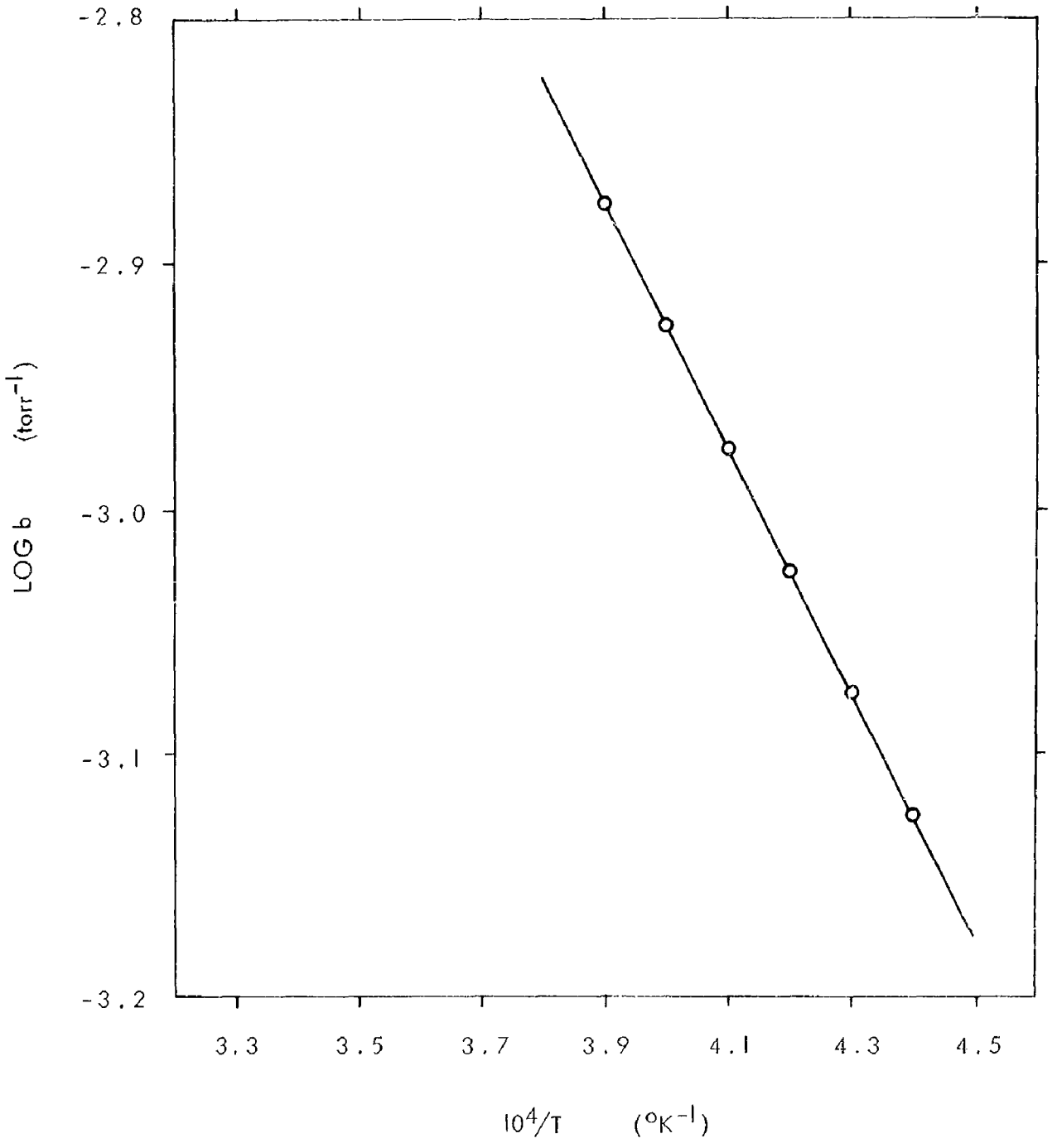

FIGURE A - 7 TEMPERATURE DEPENDENCE OF PARAMETER b

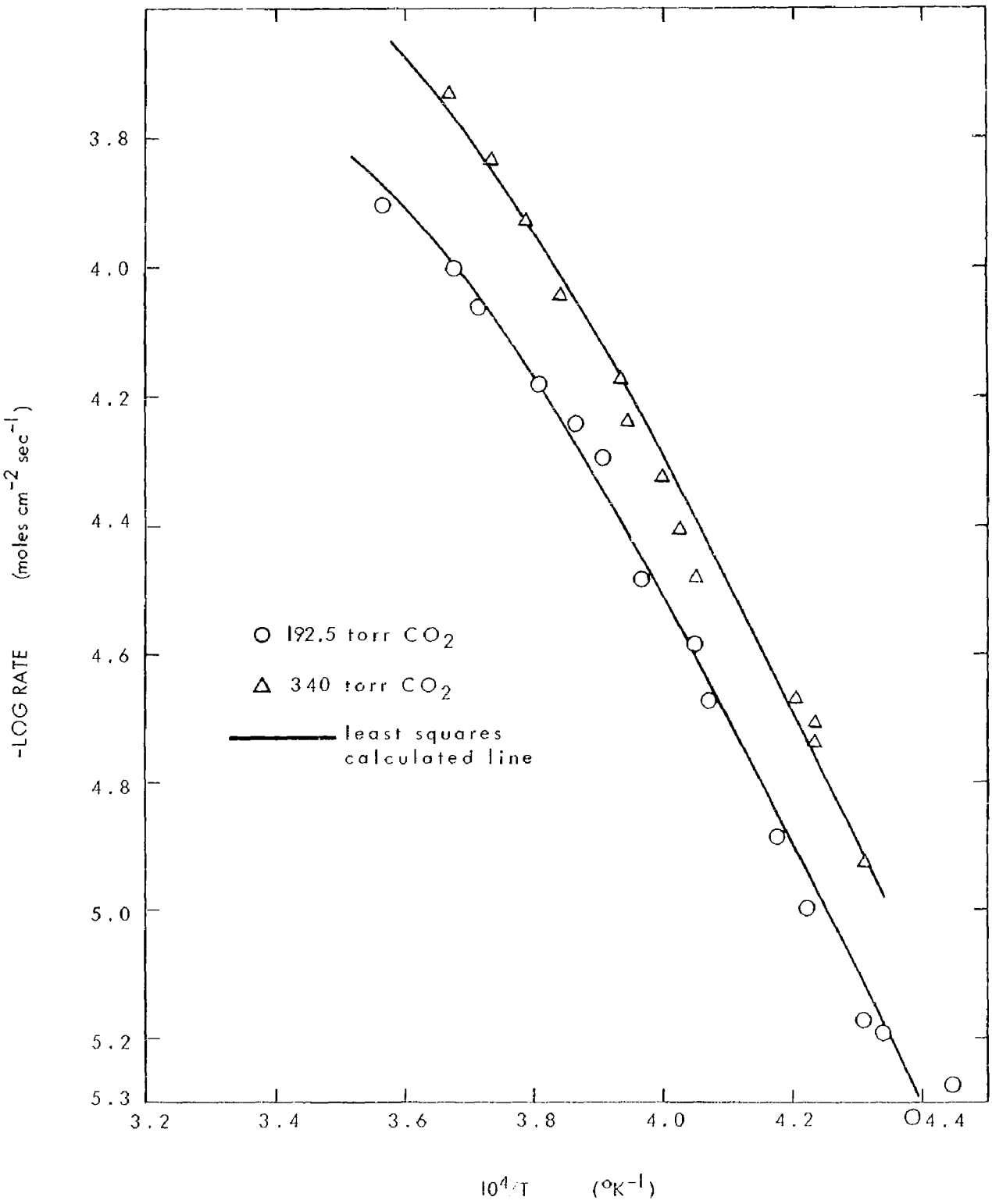

FIGURE A - 8 PRELIMINARY LEAST-SQUARES FITS AT 192.5 AND 340 TORR CO_2

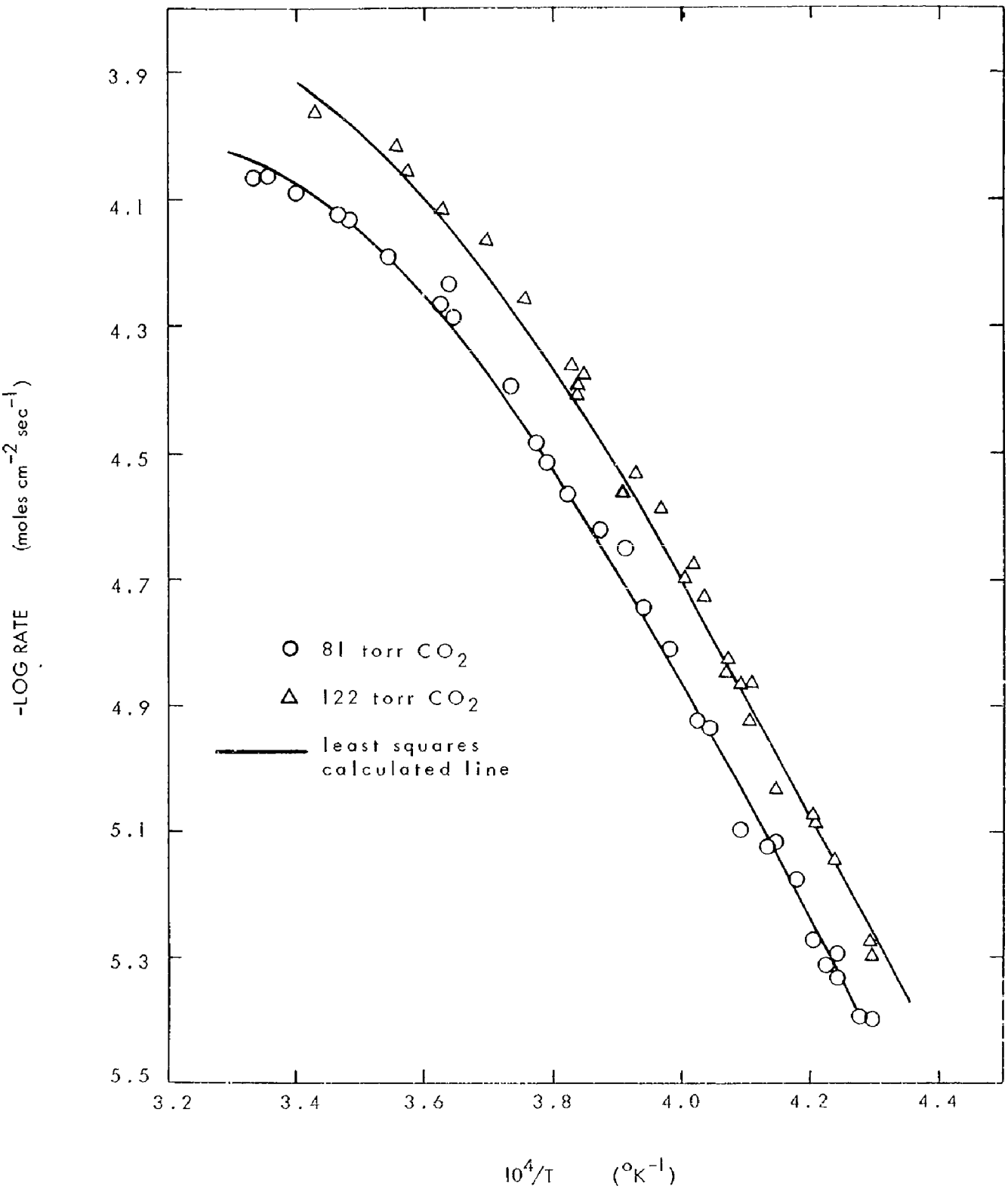

FIGURE A - 9 PRELIMINARY LEAST SQUARES FITS AT 81 AND 122 TORR CO_2

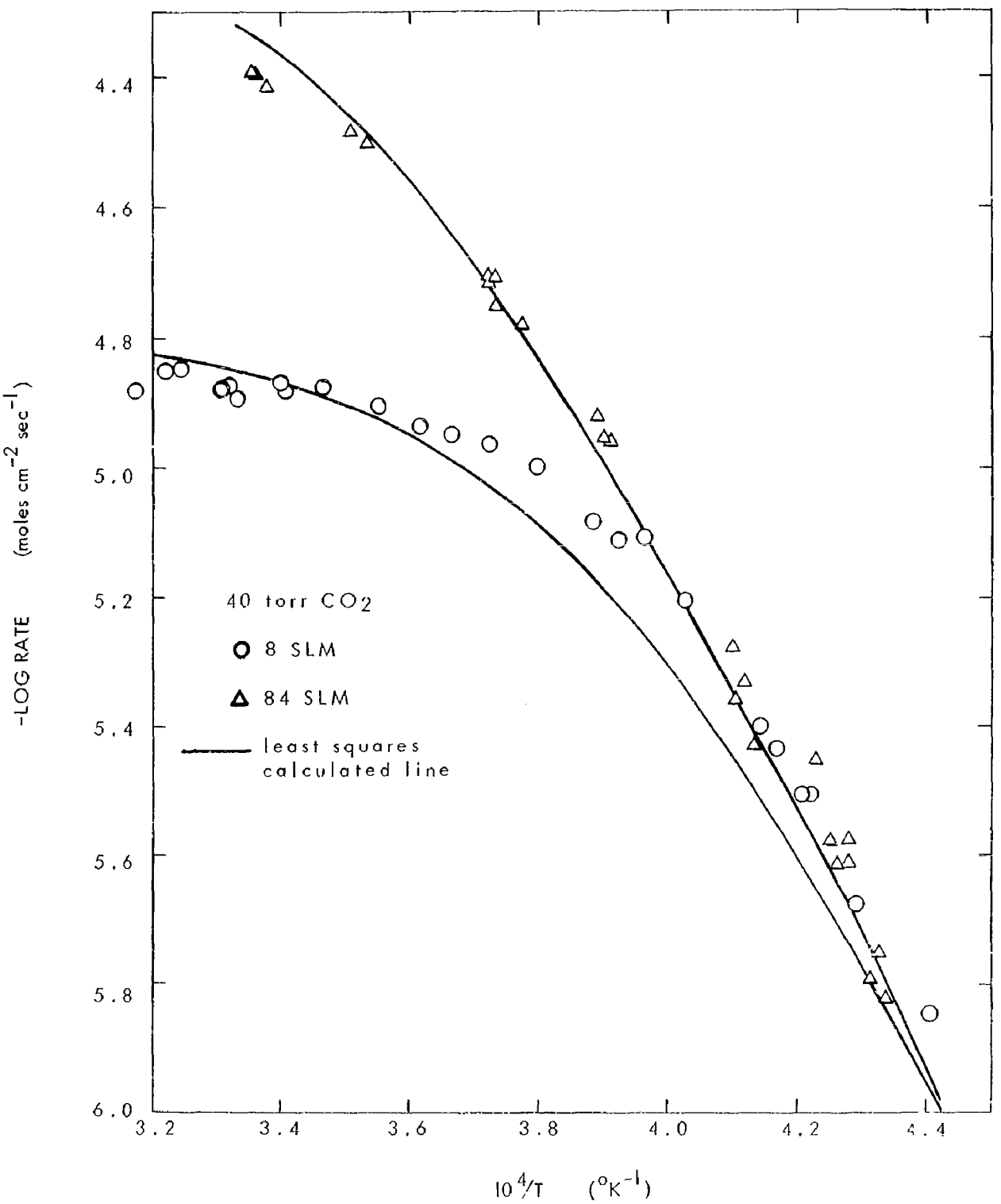

FIGURE A - 10 PRELIMINARY LEAST SQUARES FIT AT 40 TORR CO_2

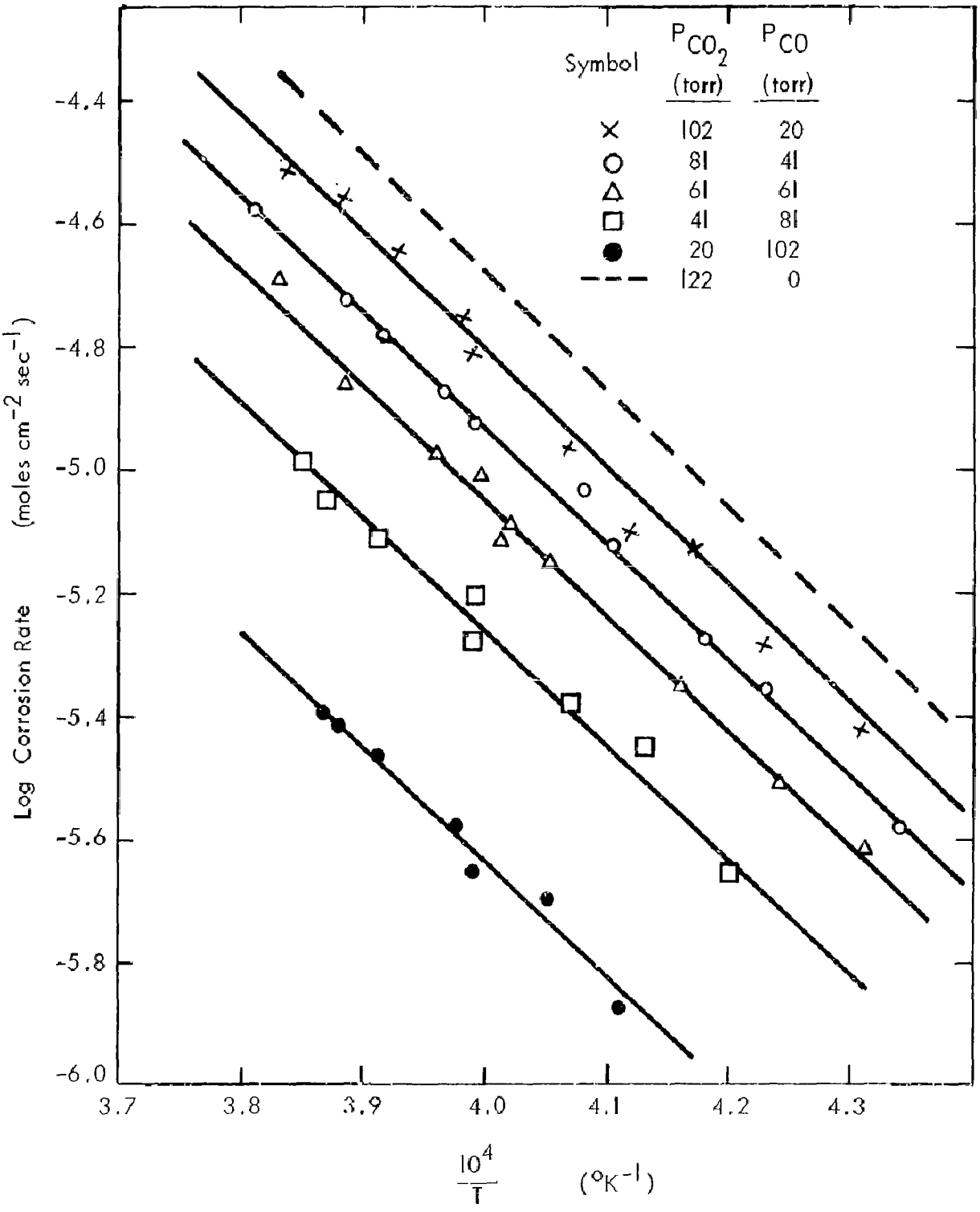

FIGURE A - II TEMPERATURE DEPENDENCE OF THE CORROSION OF W IN CO_2 - CO - Ar MIXTURES

2. High-Pressure Stagnation-Flow Reactor J.E. Smith, J.M. Quets

This induction heated reactor was described in detail previously (June, 1964 QPR). The flow measurement apparatus has been assembled and tested. Because of arcing problems, it was found necessary to maintain a nitrogen atmosphere in the region around the induction coil; the reactive atmosphere is confined to the region around the sample and the field concentrator.

The originally designed sample support, a 3" split tungsten sleeve cut from a porous tungsten bar, deteriorated rapidly in atmospheres containing CO_2 and was replaced by a 1/8" diameter tungsten rod inserted in the center of the sample bottom.

Data were taken in the 2080 to 2850°K temperature interval (Figure A-12). The flow of CO_2 from the 1/4" nozzle was 100 SLM; no argon was added. The static pressure was 1020 torr (19.7 PSIA); this corresponds to a nozzle velocity of 0.334×10^4 cm/sec and a stagnation pressure of 1033 torr. Under these conditions it was observed that the temperature dropped about 50°C during the course of an experiment (1-2 minutes) – at 200 SLM a drop of as much as 100°C in 30 seconds was observed. The temperatures plotted in Figure A-12 are estimated average temperatures; nevertheless the results are reasonably consistent. The apparent activation energy up to about 2700°K is 78 kcal/mole in reasonable accord the 86 kcal/mole obtained at lower CO_2 pressure with the low-pressure reactor.

A nozzle of smaller diameter will be tried in the hope of eliminating the temperature drops encountered at the higher flow rates and pressures. In addition, the use during the pre-reaction period of an argon flow greater than the CO_2 flow planned for the reaction period will be tried; this procedure has been successfully employed in the sub-atmospheric reactor to eliminate temperature drops.

Future Work

Study of the CO_2-W reaction will be continued to supply the data required to complement the studies described in Section A-1.

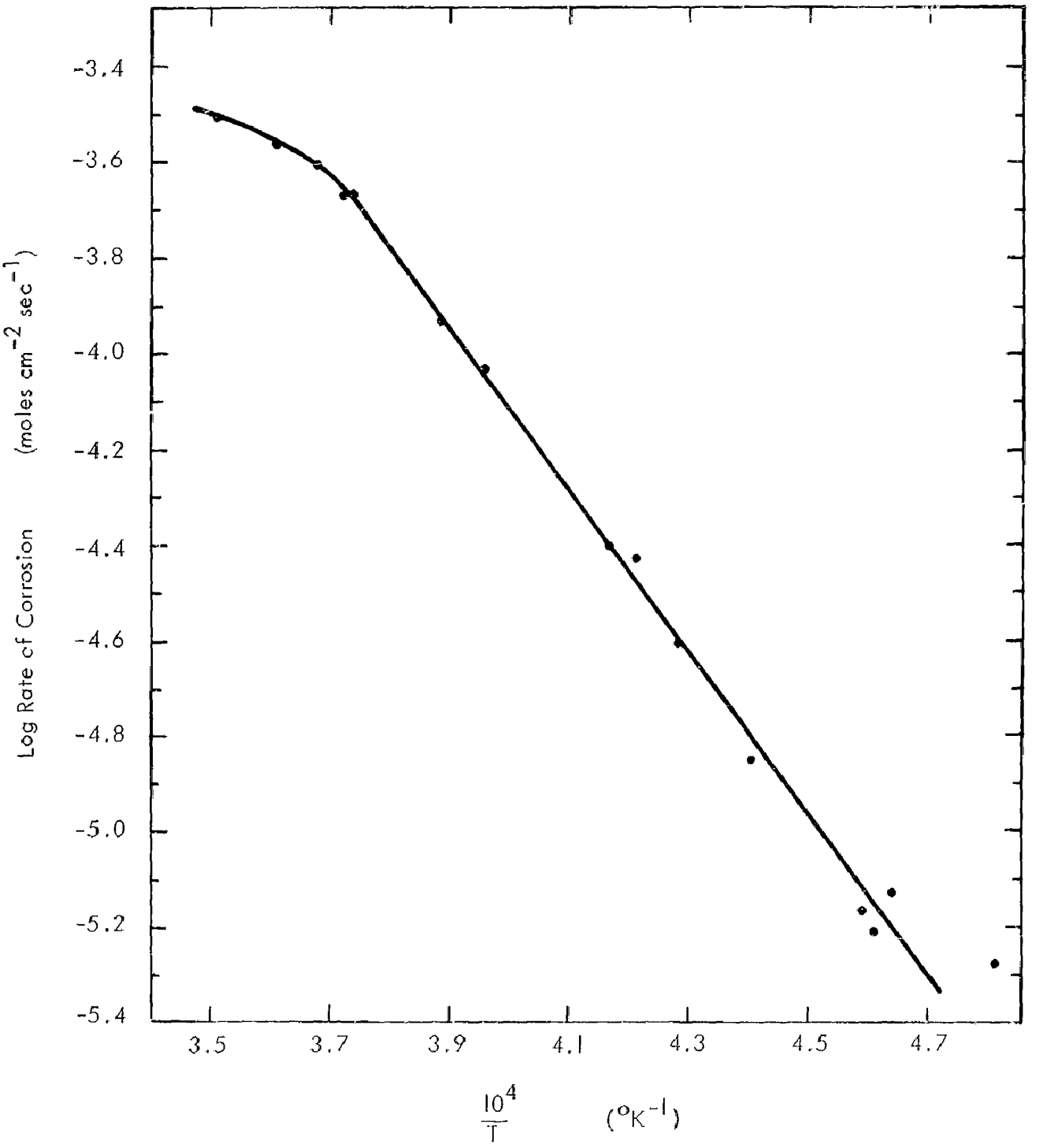

FIGURE A - 12 TEMPERATURE DEPENDENCE OF THE RATE OF CORROSION OF W BY 1033-TORR CO_2

3. Arc-Image Reactor Studies I.R. Ladd, P.N. Walsh

The study of the oxidation of 99.7% dense Linde tungsten in CO_2 using stagnation-flow geometry has been continued during this quarter. At a CO_2 partial pressure of 100 torr and a gas velocity of 9000 cm/sec, a linear relation of log corrosion rate to reciprocal temperature is found between 2200 and 2600°K (Figure A-13), consistent with data obtained at lower gas velocities in the previous quarter (June, 1964 QPR). The apparent decrease in corrosion rate with increase in gas velocity may be caused by incorrect temperature assignments as discussed below.

The temperature dependence of CO_2 attack in the predominantly surface-controlled regime has also been measured for several kinds of tungsten. The results from one fully dense and two lower density tungstens (Figure A-14), show one of the lower density tungsten to give the same rates as the high density material, while the other corrodes at rates up to twice as fast. This significant difference in reaction rate between the two low-density Rembar tungstens does not seem to be related to density, but rather to some directional structure in the original rods. The specimens of the 98.1% dense tungsten (18.90 g/cm^3) which were cut normal to the axis of the original rod, developed many deep crevices during reaction while those of the 97.4% dense material (18.75 g/cm^3), cut parallel to the rod axis, developed only a few crevices, most of which ran roughly parallel to the rod axis. Possibly during the manufacturing process networks of voids or impurities are formed that are attacked to become the crevices deeply etched into the sample. A further study of this point will be made with pieces of the same cylinder cut in both orientations. The above experiments suggest that under practical engineering conditions, the apparent oxidation rate of tungsten in CO_2, in the surface-controlled regime, may vary significantly according to the manufacture of the material.

The attack manifested upon large grain, fully-dense tungsten*, Figure A-15, is substantially different from the attack previously observed upon small grain, less dense tungsten. The polished front surface of the arc-melted

---

* The fully-dense tungsten, [illegible] supplied by F. G. Keith, was cut [illegible] in the same direction.

samples remained quite smooth. At 2500-2600°K the main topological feature of interest was the appearance of etch pits, some quite large. At 2300°K the etch pits were smaller and less prominent, and an intragranular terracing effect became the predominant feature. All the arc-melted samples remained well enough polished that the emittance, measured as described below, did not change significantly during reaction. The last picture in Figure A-15 shows the oxidized surface of tungsten plated on tungsten using fused salt technique. Although after oxidation the surface was rougher than the arc-melted tungsten, it remained substantially more reflective than the less than fully-dense tungsten. The oxidation rate of this one sample fell on the line generated in Figure A-14 by the arc-melted tungsten.

The severe erosive attack upon the Rembar tungsten made it necessary to measure emittance values in order to determine the true temperatures. The tungsten pieces for which data are shown in Figure A-14 were polished on the front surface before reaction to remove marks introduced during preparation; the temperature corrections applied were based upon emittances measured by re-polishing one-half of the reacted surface and then comparing the brightness temperatures of the repolished and unpolished halves while heating the sample in argon. Assuming emissivity of 0.44 for the polished half, the emittance of the unpolished half was calculated from the apparent difference in temperature of the two halves. The emittances of the 98.1% and 97.4% dense Rembar tungsten varied between 0.86-0.99 and 0.46-0.64 respectively. The very high emittances were probably caused by the network of deep crevices eroded into the front faces of these samples.

Emittance determinations were not made on the samples represented in Figure A-13 even though microscopic examination of the surfaces after reaction (Figure A-16) shows that at the same brightness temperature they were rougher after reaction at 9000 cm/sec than at 2000 cm/sec. The temperature uncertainty introduced by not correcting for emittance is much less with the 99.7% dense Linde tungsten than would have been the case with the less dense Rembar tungstens.

Equipment for using HF as the reactive component of the gas has been assembled and tested. Experimental difficulties still exist but some data should be forthcoming next quarter.

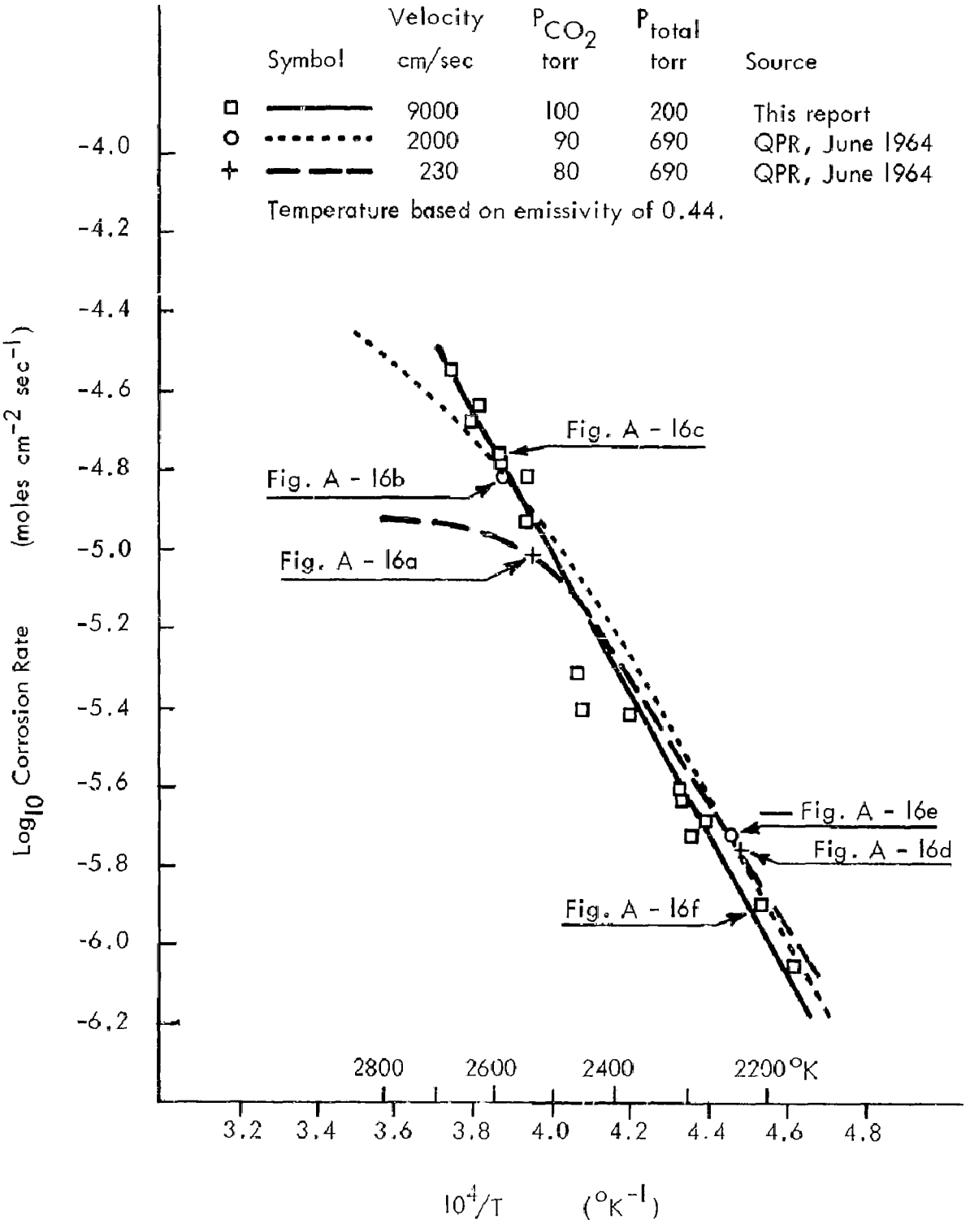

FIGURE A - 13 TEMPERATURE DEPENDENCE OF THE CORROSION RATE OF LINDE TUNGSTEN IN CO_2

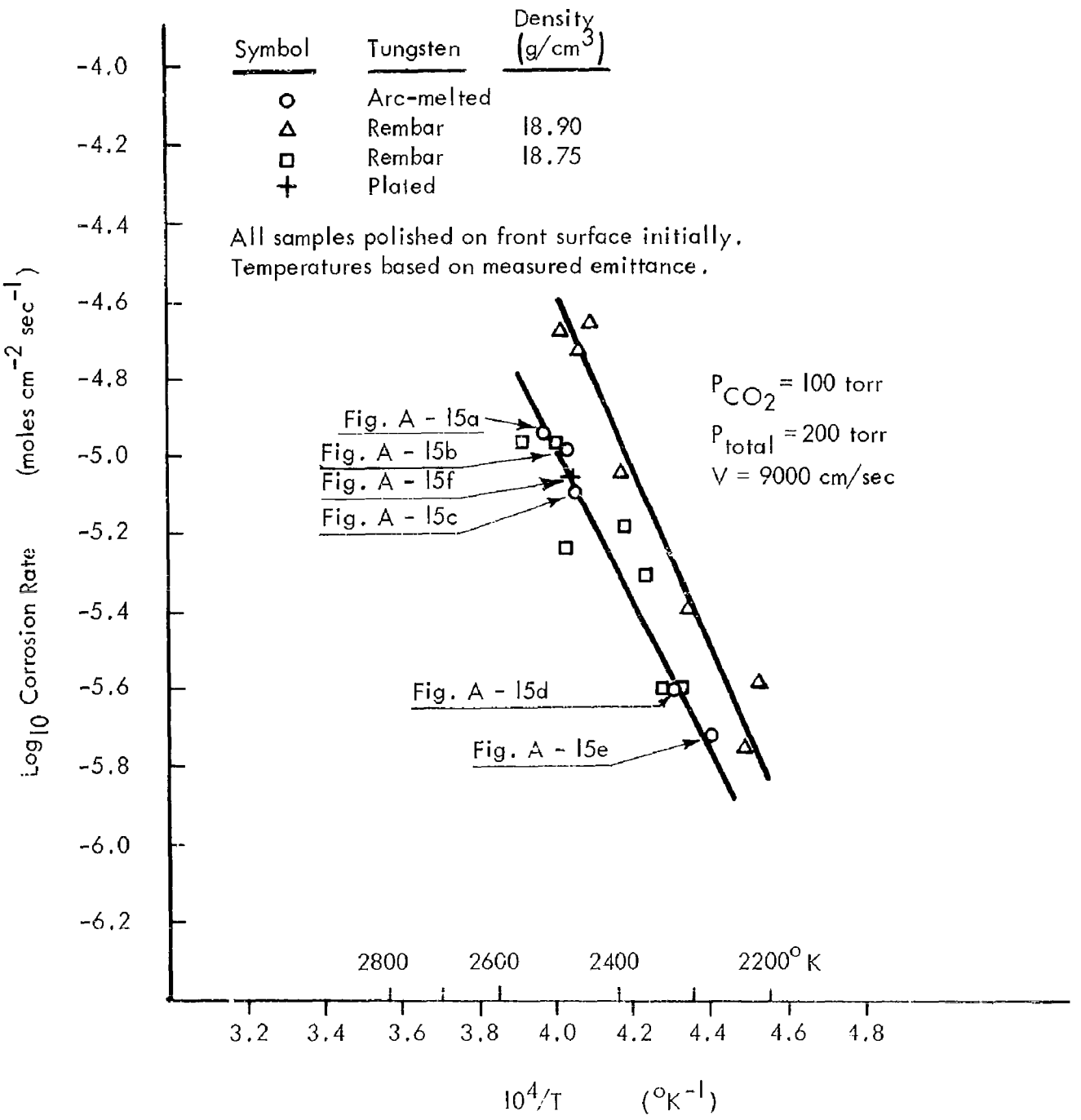

FIGURE A - 14 TEMPERATURE DEPENDENCE OF THE CORROSION RATE OF SEVERAL TUNGSTEN SAMPLES IN CO_2

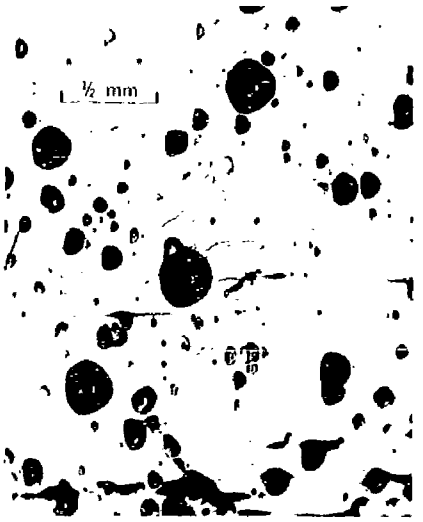

a. Arc-melted 2520°K

b. Arc-melted 2480°K

c. Arc-melted 2470°K

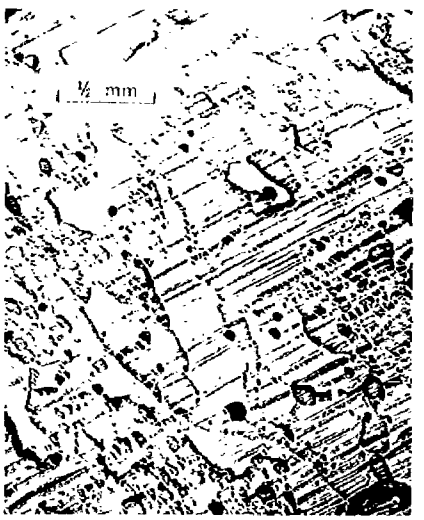

d. Arc-melted 2325°K

e. Arc-melted 2275°K

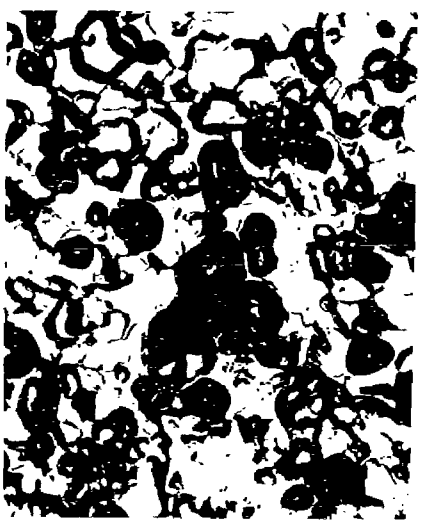

f. W Plated on W 2470°K

FIGURE A - 15 OXIDIZED SURFACES OF FULLY DENSE TUNGSTEN AFTER 3.0 MINUTES EXPOSURE TO 100 TORR CO_2 FLOWING AT 9000 CM/SEC.

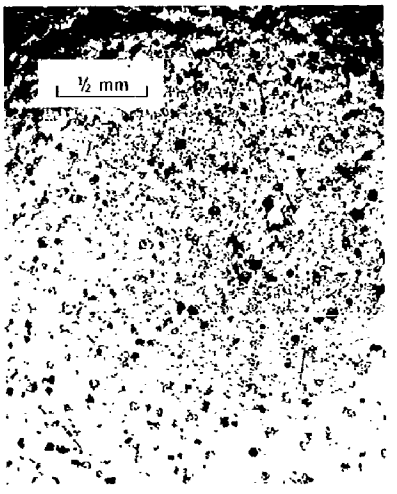

a. 2530°K, 80 torr CO_2
230 cm/sec

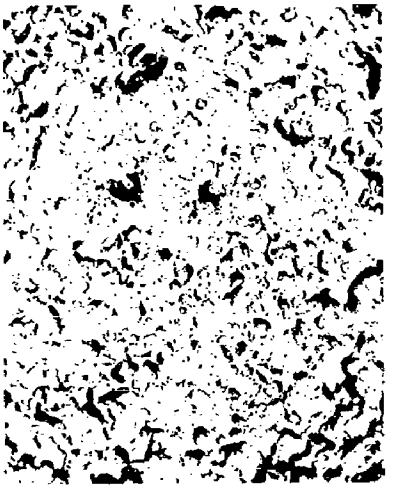

b. 2580°K, 90 torr CO_2
2000 cm/sec

c. 2585°K, 100 torr CO_2
9000 cm/sec

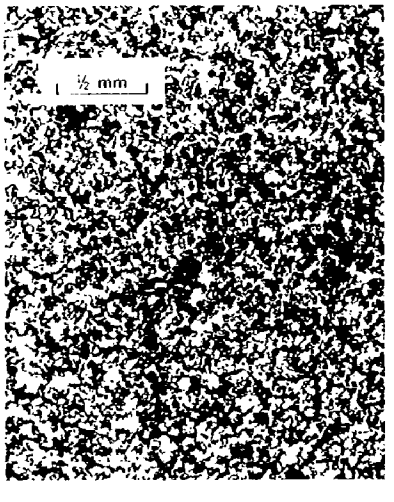

d. 2230°K, 80 torr CO_2
230 cm/sec

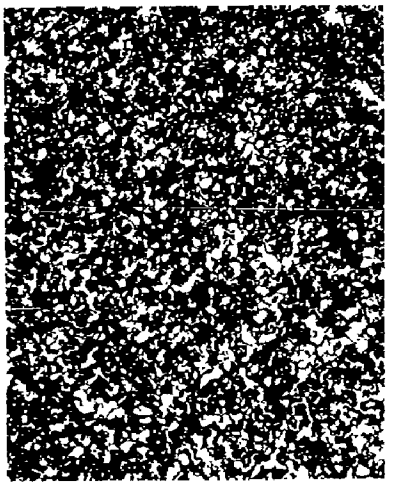

e. 2240°K, 90 torr CO_2
2000 cm/sec

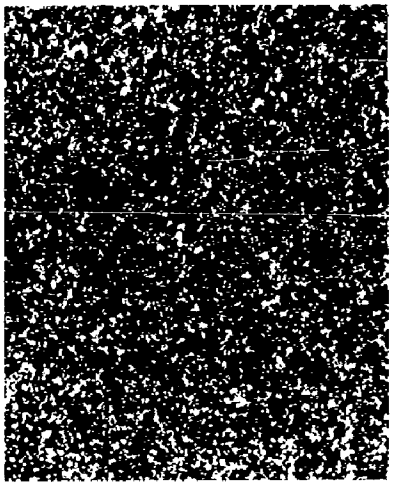

f. 2200°K, 100 torr CO_2
9000 cm/sec

FIGURE A - 16 OXIDIZED SURFACE OF 99.7% DENSE LINDE TUNGSTEN AFTER 3.0 MINUTES EXPOSURE TO 80-100 TORR CO_2 FLOWING AT THREE VELOCITIES.

The approach taken to the treatment of stagnation-flow reactors was described in the March, 1964 QPR, p. III-23 ff. In the solution to the external flow problem given there, compressibility effects were included as a perturbation, to the first order, to the velocity potential for an incompressible fluid. The solution has been extended to the second order during this quarter.

Differential equations for the stagnation line in the boundary layer were given in the June, 1964 QPR (p. III-30 ff.). During this quarter, a computer program for the numerical solution of these differential equations, along with auxiliary subroutines required for the estimation of the physical properties of the gas mixtures, has been written and tested.

The Exterior Flow Problem. - The Rayleigh-Janzen method (March, 1964 QPR, p. III-24 ff.) has been carried to the second perturbation order. The resulting velocity distribution is

$$\frac{V_r}{V_1} = \frac{r}{2} + M_1^2 \left(\frac{r^2}{16} - \frac{1}{3}\right) \frac{r}{2} + M_1^4 \left[\left(\gamma + \frac{3}{2}\right) \frac{r^4}{24} - \frac{2\gamma+1}{16} r^2 + \frac{\gamma-1}{5} + \frac{\gamma-1}{8} \left(-\frac{7}{30} + z^2 - \frac{z^4}{2}\right)\right] \frac{r}{6} \quad (4)$$

$$\frac{V_z}{V_1} = -z + M_1^2 (1-z^2) \frac{z}{3} + M_1^4 \left[\frac{\gamma-1}{2} (1-z^2) r^2 - (23\gamma + 57) \frac{z^4}{10} + (11\gamma + 13) \frac{z^2}{3} - \frac{41}{30} (\gamma-1)\right] \frac{z}{24} . \quad (5)$$

The details of solution will be presented in a technical report to be issued in the next month.

Certain results given in March, 1964 QPR have been found to be in error. On p. III-28 and 29, Eqns. 24, 26, and 27-29 should be corrected to read

$$\phi_1 = \frac{1}{3}\left(\frac{z^2}{2} - \frac{z^4}{4}\right) + \frac{r^4}{128} - \frac{r^2}{12} \tag{24}$$

$$\frac{V_z}{V_1} = \left[\, 1 - \frac{1}{3} M_1^2 \,(1-z^2)\right] z \tag{26}$$

$$\frac{dr}{dz} = \frac{V_r}{V_z} = - \frac{\left[1-M_1^{\,2}\left(\frac{1}{3} - \frac{r^2}{16}\right)\right] r}{2\left[1 - \frac{1}{3} M_1^{\,2}\,(1-z^2)\right] z} \tag{27}$$

$$\frac{z}{z_1} \frac{\left[\frac{M_1^{\,2}}{3}\,(1-z_1^{\,2})-1\right]^{\frac{1}{2}}}{\left[\frac{M_1^{\,2}}{3}\,(1-z^2)-1\right]^{\frac{1}{2}}} = \frac{r_1^{\,2}}{r^2} \frac{1 - \frac{M_1^{\,2}}{3} + \frac{M_1^{\,2}}{16} r^2}{1 - \frac{M_1^{\,2}}{3} + \frac{M_1^{\,2}}{16} r_1^{\,2}} \tag{28}$$

$$z = z_1 \left(\frac{r_1}{r}\right)^2 \tag{29}$$

hese changes have a small effect on Figs. A-15 and A-16 but do not modify the conclusions expressed on p. III-29 regarding streamlines and velocity distributions.

Estimation of Physical Properties. - The differential equations describing the boundary layer region (June, 1964 QPR, Table A-11) require expressions for mixture physical properties in terms of temperature, pressure, and composition. The expression

$$C_{P_i} = a_i + b_i T + \frac{c_i}{T^2} \tag{1}$$

was adopted for the heat capacity and the constants evaluated for individual species by the method of least squares from data tabulated in reference 1. To estimate transport properties, we have chosen the kinetic theory expressions

---

1. JANAF Thermochemical Tables, Dow Chemical Co., Midland, Michigan.

as quoted by Brokaw.[2] Tables of collision integrals[3] for these expressions have been reduced to polynominals in $\ell n\ T^*$ (using the nomenclature of reference 2). The results are

$$\Omega^{(2,2)^*} = 1.58378 - 0.71595\ (\ell n\ T^*) + 0.24702\ (\ell n\ T^*)^2 - 0.041956\ (\ell n\ T^*)^3 + 0.0025925\ (\ell n\ T^*)^4, \qquad (2)$$

for the viscosity and thermal conductivity, and

$$\Omega^{(1,1)^*} = 1.44174 - 0.67270\ (\ell n\ T^*) + 0.25154\ (\ell n\ T^*)^2 - 0.047295\ (\ell n\ T^*) + 0.0032282\ (\ell n\ T^*)^4, \qquad (3)$$

for the diffusivity. These equations reproduce the tables with a maximum deviation of 3% above $T^* = 0.4$.

Computer subroutines for the calculation of the mixture transport properties were prepared for use with the program for solving the stagnation-line equations.

Numerical Solution of Approximate Stagnation-Line Equations. - A program was written for the numerical solution of the stagnation-line equations by forward integration from assumed conditions at the solid surface. This program employs a library routine based on the Runge-Kutta and Adams Methods. For use with this routine, the differential equations were expanded, by the introduction of new dependent variables, to a system of first order equations.

---

2. R. S. Brokaw, Technical Report R-81 National Aeronautics and Space Administration (1961).
3. J. O. Hirschfelder, C. F. Curtiss, and R. B. Bird, Molecular Theory of Gases and Liquids, Table I-M, p. 1126-7, John Wiley and Sons, Inc. (1954).

Tests of this program showed that the integration scheme, as written, was unstable. Steps to remove the instability are being explored.

Future Work. - The exterior flow solution is now available up to the second perturbation. This is expected to provide sufficient accuracy and no further work on the external solution is planned. Since the computer program prepared to solve the boundary layer equations has proved unstable, it will be modified.

5. Mass-Spectrometric Studies O.C. Trulson & P. Schissel

a. Tungsten-Oxygen System — Sticking Probability

From a variety of measurements on the pressure and temperature dependences of the products of the tungsten-oxygen reaction a plausible kinetic model has been deduced which fits the experimental data. The model involves two distinct types of sites for oxygen adsorption, the first characteristic of bare tungsten and the second of a surface already covered with a monolayer of oxygen. The observation that nearly every O_2 molecule impinging upon bare tungsten at 2900°K dissociates to 2 O(g) indicated that the sticking probability for O_2 on the first type of adsorption site is nearly unity and led us to set this parameter of the model equal to unity for all temperatures. No direct test similar to this was available for the sticking probability on the second type of adsorption site, but it was also set equal to unity. A direct experiment has now been performed that bears on the sticking probability on the second layer.

The experimental arrangement is shown in Figure A-17. Two independently heated filaments were mounted facing each other on a moveable platform such that either filament could be positioned under the shutter-slit entrance to the mass spectrometer. Filament f_1 was heated to 2600°K in ambient oxygen and the atomic oxygen produced was measured directly from the top surface of this filament. The platform was then moved to position filament f_2 under the shutter slit, the filament was heated, and the products from f_2 were observed (WO_2, WO_3, O, W_2O_6, W_3O_9). Because of the close proximity of the two filaments (0.040"), a large fraction (approximately one-third as determined by measuring the O(g) which is produced by f_1 and reflected from f_2 when f_2 is not heated) of the products from f_1 impinged upon f_2. With f_1 at 2600°K the principal product of reaction is atomic oxygen, confirmed by the direct measurement above. No significant difference in the rate of production of WO_2, WO_3, W_2O_6, and W_3O_9 was observed from the second filament at any temperature with f_1 on or off, which, in terms of the kinetic model, implies that the sticking probability on the second type of adsorption site is independent of whether atomic or molecular oxygen is the impinging gas. Since one would expect a high sticking coefficient for atomic oxygen these observations confirm the high sticking probability for O_2 on the second type of adsorption site that was assumed in our previous calculations.

b. Other Systems

The measurements on tungsten-oxygen are essentially completed and have been followed by a number of qualitative observations on other systems prior to more detailed studies of the more interesting ones.

1) Nb-O_2 and Ta-O_2

Copious amounts of NbO(g), NbO_2(g), TaO(g), and TaO_2(g) were observed, but no O(g). The oxide signals in addition to being dependent on pressure and temperature, were time-dependent. It is presumed that this time dependence is due to diffusion of oxygen into the solid phase.

2) W-CO and W-CO_2

Preliminary to running CO_2, tungsten was heated in the presence of CO. At 2500°C brightness temperature only trace amounts of O(g) and C(g) were observed and no tungsten oxide signals were detected at any temperature. It is concluded that while CO might inhibit reaction of CO_2 by virtue of interaction on the surface, the direct products from CO will be nil.

Studies of the reaction of CO_2 with tungsten were begun and are complicated from the experimental standpoint when compared to the O_2-W system because the oxide products are less abundant while CO and O_2(g), which can cause secondary reactions, are found in relatively large amounts. The first measurements at about 2800°K indicate that O(g) is formed from CO_2 in an abundance comparable to that from O_2(g). Small amounts of WO_2 and WO(g) are observed, but WO_2(g) is less abundant than WO(g), while the reverse is true for the O_2 reaction.

3) Mo-O_2

Results of measurements on this system, currently underway, were expected to be similar to those from the W-O reaction. Qualitatively this is not copious amounts of O(g), MoO_2(g), and Mo_2O_5(g) are observed. However, MoO(g) is observed in relatively large abundance compared to the WO from the O_2-tungsten reaction.

c. Future Work

It is planned to continue with detailed measurements of the temperature and pressure dependences of the species observed with the Mo-O_2 system and with further exploratory measurements on the CO_2-W system.

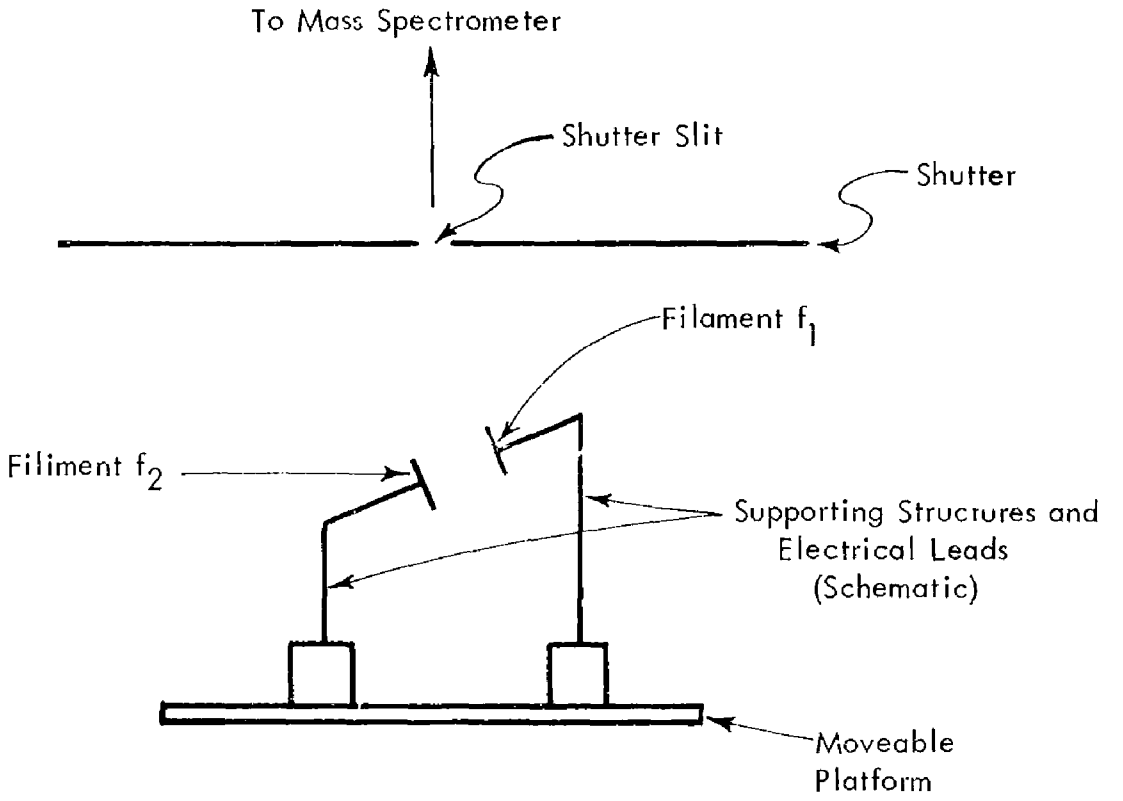

FIGURE A - 17 SCHEMATIC VIEW OF APPARATUS USED FOR REACTION OF ATOMIC OXYGEN AND TUNGSTEN

6. Rocket-Nozzle-Insert Test-Analysis Program — R.I. Gray

A new high pressure liquid motor for insert corrosion prediction studies (as discussed in June, 1964 QPR) is being designed and will be built by the Propulsion Laboratory, Directorate of Research and Development, Army Missile Command, Huntsville, Alabama. Design details on the test tungsten nozzle inserts have not yet been furnished us so the inserts are still to be fabricated.

On the assumption that the nozzle insert outside diameter would not exceed 1-1/2 inches full density tungsten rod of this diameter has been obtained from General Electric. Samples of this tungsten rod are being prepared for testing in the arc-image furnace to compare its reaction rates with those obtained with other full density tungstens.

It seems certain that reaction rate kinetics at the nozzle insert will influence the reaction rate of the tungsten insert during the motor firing period. To calculate the quantitative effects of reaction kinetics on insert recession rate it is necessary to know the insert surface temperature history during the motor firing. A number of calculations have therefore been carried out on a geometry which approximates the nozzle insert dimensions anticipated for the motor test program. The initial calculation assumed a UDMH-N_2O_4 (36-62 wt.%) combustion mixture at a chamber pressure of 1000 psi. T. thoat diameter was assumed to be 1/2" inch and the outside insert diameter to be 1-1/2". Heat transfer coefficients were estimated from the simplified Bartz equation with all physical properties evaluated at film temperature conditions. The temperature transients within the insert materials were calculated from temperature tables for the one-dimensional, one-layer cylindrical shell*. It was assumed that the outside surface of the insert would be adiabatic. From these calculations it was possible to obtain the nozzle insert surface temperature history for the case of a non-receding interface. In addition, the time dependent temperature gradients within the insert material were also obtained.

With these calculations it will be possible to determine the total surface recession rate and surface position as a function of time. From these data thermocouple placements for the appropriate measurement of the nozzle in-

---

* Temperature Tables, Part 2, C. J. Thorne, H. C. Morris, NAVORD report 1762, 15 March 1961.

sert interior temperatures can be obtained. In addition, knowledge of the temperature gradients within the insert materials will make possible estimates of the elastic thermal stresses generated in the insert. Mechanical failure of the nozzle insert thus may be anticipated.

B. Physical and Mechanical Properties

1. High-Temperature X-ray Studies — F. G. Keihn

Our least-squares program for computing the lattice parameters of a crystal from observations of the (indexed) diffraction pattern of a powder sample, described in previous quarterly reports, has been studied further and checked using a standard tungsten powder sample obtained from W. Parrish (Acta Cryst. 13, 838 (1960)). The results from four runs on the Siemens diffractometer are given in Table B-I. The program corrected the lattice constant for the errors from the flat-specimen geometry and for the specimen-displacement from the diffractometer axis. The values obtained are in excellent agreement with the average of the values obtained by 10 laboratories in Parrish's study. The values obtained by the center-of-gravity method are consistently low by about 0.00034 Å: our techniques of measuring the centers of gravity must introduce a systematic error. The α_1 peaks are the sharpest and probably allow for better determination of peak value. The average of the α_1 values agrees with Parrish's published value within $\frac{1}{2}\sigma$ (0.00005 Å). Therefore, this method will be used for our lattice constant measurements unless there are too few resolved $\alpha_1\alpha_2$ peaks. In this case the center-of-gravity method will have to be used.

In the study of the thermal expansion of NbB_2 and TaB_2, it has been found that NbB_2 and TaB_2 lose boron when heated to temperatures of 1200°C and above. With one NbB_2 specimen the boron depletion on the surface was so great that only lines of Nb_3B_4 and NbB were obtained. Since the lattice constant of NbB_2 varies with the boron content, the thermal expansion can only be measured by this method if the initial room temperature lattice constant agrees with room temperature lattice constant after the thermal expansion run.

This boron depletion was observed on samples of NbB_2 heated in other vacuum furnaces. Only when NbB_2 was heated in an argon atmosphere in a carbon tube furnace in which boron was placed in a crucible with the sample, was the sample unchanged after heating to temperatures as high as 2000°C.

Attempts to stabilize the NbB_2 phase by coating the surface with a layer of boron through which diffraction of NbB_2 could be observed were unsuccessful. New samples of NbB_2 and TaB_2 with excess boron are being prepared and will be tried. Also the vacuum furnace for the diffractometer has been

modified for a helium atmosphere which should decrease the rate of evaporation of boron.

A TiB_2 specimen was obtained, and the thermal expansion measured with the diffractometer furnace. The data were processed by the least-square program and are compared with our previous data in Table B-II. The agreement is fairly good considering that the new results are from a new TiB_2 sample. It also indicates little or no boron loss up to these temperatures.

Future Work. - The effect of specimen displacement on lattice constant will be checked against the tungsten standard by arbitrarily displacing the specimen from the diffractometer axis. The loss in boron of TiB_2 and ZrB_2 at higher temperatures will be determined. The thermal expansion of NbB_2 and TaB_2 doped with excess boron will also be determined both in vacuum and with a helium atmosphere.

Table B-1

Lattice Parameters of Tungsten (Parrish) at 25°C

Run	Method		Lattice Constant Å	σ
1	$CuK\alpha_1$	peaks	3.16516	8.0×10^{-5}
1	$CuK\alpha_2$	"	3.16500	3.3×10^{-5}
1	$CuK\alpha_1\alpha_2$	center of gravity	3.16479	5.9×10^{-5}
2	$CuK\alpha_1$	peaks	3.16506	8.9×10^{-5}
2	$CuK\alpha_2$	"	3.16491	3.5×10^{-5}
3	$CuK\alpha_1$	"	3.16530	1.7×10^{-5}
3	$CuK\alpha_2$	"	3.16514	6.4×10^{-5}
4	$CuK\alpha_1$	"	3.16519	11.3×10^{-5}
4	$CuK\alpha_2$	"	3.16513	4.2×10^{-5}
4	$CuK\alpha_1\alpha_2$	center of gravity	3.16496	4.0×10^{-5}
		Total average	3.16506	15.0×10^{-5}
		Average of peaks	3.16511	12.0×10^{-5}
		Average of α_1 peaks	3.16518	9.9×10^{-5}
		Average of cg.	3.16488	12.0×10^{-5}
W. Parrish, Acta Cryst. 13, 838 (1960)			3.16522 ± 0.00009Å	

* All lattice constants corrected for refractive index.

Table B-II

Lattice Parameters for TiB_2 vs Temperature

Temp.	a(Å)	$\sigma \times 10^4$ *	C(Å)	$\sigma \times 10^4$ *	$\frac{\Delta a}{a}\ 10^3$	$\frac{\Delta C}{C}\ 10^3$	Method
25	3.0293	1.8	3.2288	1.3			new
750	3.0438	3.4	3.2486	2.5	4.82	6.26	new
1000	3.0496	3.3	3.2587	2.4	6.73	9.39	new
1250	3.0554	6.1	3.2670	4.5	8.62	11.96	new
25	3.0291	2.1	3.2280	1.5			new
25	3.0286		3.2282				old
754	3.0418		3.2482		4.39	6.19	old
1012	3.0486		3.2589		6.64	9.50	old
1260	3.0556		3.2678		8.91	12.26	old

* σ's for new method are from least-square program for individual measurements. No σ's for the old method were quoted by Houska (September, 1963 QPR).

2. Elastic Properties

R. Lowrie

The velocities of shear and compressional waves in polycrystalline tungsten have been measured from 24° to 1800°C. An ultrasonic pulse-echo technique was used to determine the difference in transit time for waves reflected from the specimen shoulder and from the end of the sample (Figure B-1). From this time Δt and the shoulder-to-end length $\ell_o/2$, the velocity of the wave, shear v_s or compressional v_c, may be computed; and from these velocities one computes the shear modulus G and the infinite-medium compressional modulus L by $G = \rho v_s^2$ and $L = \rho v_c^2$, where ρ is the density.

The specimen, of commercial tungsten purchased from the General Electric Company, had a density of 19.15 ± 0.01 g/cc as determined from its weight and dimensions. This is 99.4% of the theoretical density of 19.265 g/cc. As the specimen is heated, both the density and the shoulder-to-end length change. The net result of both effects on the modulus is given in the following equation, where the subscripts o and T represent values at room and elevated temperatures respectively:

$$G_t = \rho_t\left(\frac{\ell_t}{\Delta t_s}\right)^2 = \rho_o\left(1 + \frac{\Delta\ell}{\ell_o}\right)^{-3} \cdot \left(\frac{\ell_o}{\Delta t_s}\right)^2\left(1 + \frac{\Delta\ell}{\ell_o}\right)^2 = \frac{\rho_o \ell_o^2}{\Delta t_s^2}\left(1 + \frac{\Delta\ell}{\ell_o}\right)^{-1},$$

and similarly

$$L_t = \frac{\rho_o \ell_o^2}{\Delta t_c^2}\left(1 + \frac{\Delta\ell}{\ell_o}\right)^{-1}.$$

The values of Jones and Langmuir[1] and Houska[2] for the thermal expansion of tungsten essentially coincide up to 1400°C. Above this Houska's values, which have been used here, are slightly lower. The difference reaches 0.02% (0.93% expansion compared to 0.95%) at 1800°C.

---

1. H. A. Jones and I. Langmuir, General Electric Review 30, 310-319, 354-362, and 408 (1927), data in Handbook of Chemistry and Physics, Chemical Rubber Publishing Company.

2. C. R. Houska, J. Phys. Chem. Solids 25, 359 (1964).

The experimental values for G and L, determined using both quartz and PZT-4 transducers, are given in Figures B-2 and B-3. The results previously reported by Bernstein[3] and obtained with the same basic equipment are also shown on Figures B-2 and B-3. The agreement is generally good except for the somewhat peculiar behavior of Bernstein's G values above 600°C.

Values of G and L were taken every hundred degrees from the curve drawn as a best fit for the experimental points, and these values were used to calculate the Young's modulus E, bulk modulus K, and Poisson's ratio σ at each temperature (Figures B-4, B-5, and B-6) by the elastic relations $E = \frac{G(3L-4G)}{(L-G)}$, $K = \frac{3L-4G}{3}$, and $\sigma = \frac{L-2G}{2(L-G)}$.

The results of Hill and Shimmin[4] for E from room temperature to 760°C are also plotted in Figure B-4 after correction for the effects of thermal expansion on sample length and density. Hill and Schimmin report a specific gravity of 19.154 for their tungsten sample. The general agreement for E is quite good.

Tungsten crystal L-2 has been successfully bonded to a tungsten buffer rod, and it appears that satisfactory data for C_{11} as a function of temperature can be obtained from it. Such results plus the data previously obtained for C_{44} and C_N ($= \frac{1}{5} C_{11} + \frac{2}{5} C_{12} + C_{44}$) (Quarterly Progress Report, June 1964) will yield the individual values of C_{11}, C_{12}, and C_{44} as functions of temperature to 1800°C.

Future Work. The above-mentioned measurements of C_{11} will be made to 1800°C. The values for C_{11}, C_{12}, and C_{44} will be used to calculate the elastic constants of polycrystalline tungsten, and these will be compared with the experimental values reported this quarter. Reports of this work will be written for publication.

---

3. B. T. Bernstein, J. Appl. Phys. 33, 2140 (1962).

4. W. H. Hill and R. B. Schimmin, "Elevated Temperature Dynamic Elastic Moduli of Various Metallic Materials", WADD TR 60-593, March 1961, AD 254825.

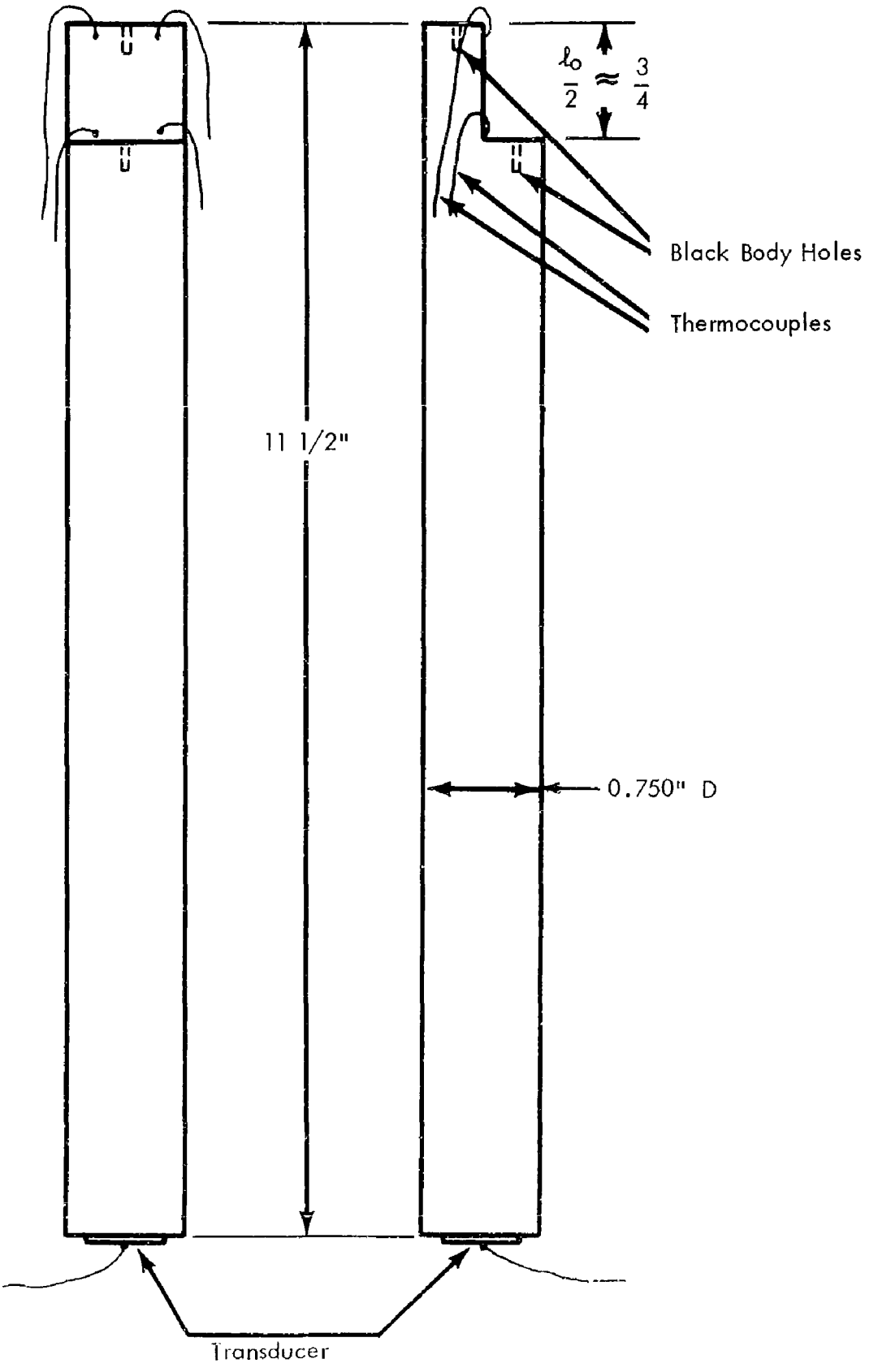

FIGURE B - 1 SAMPLE FOR MODULUS DETERMINATION

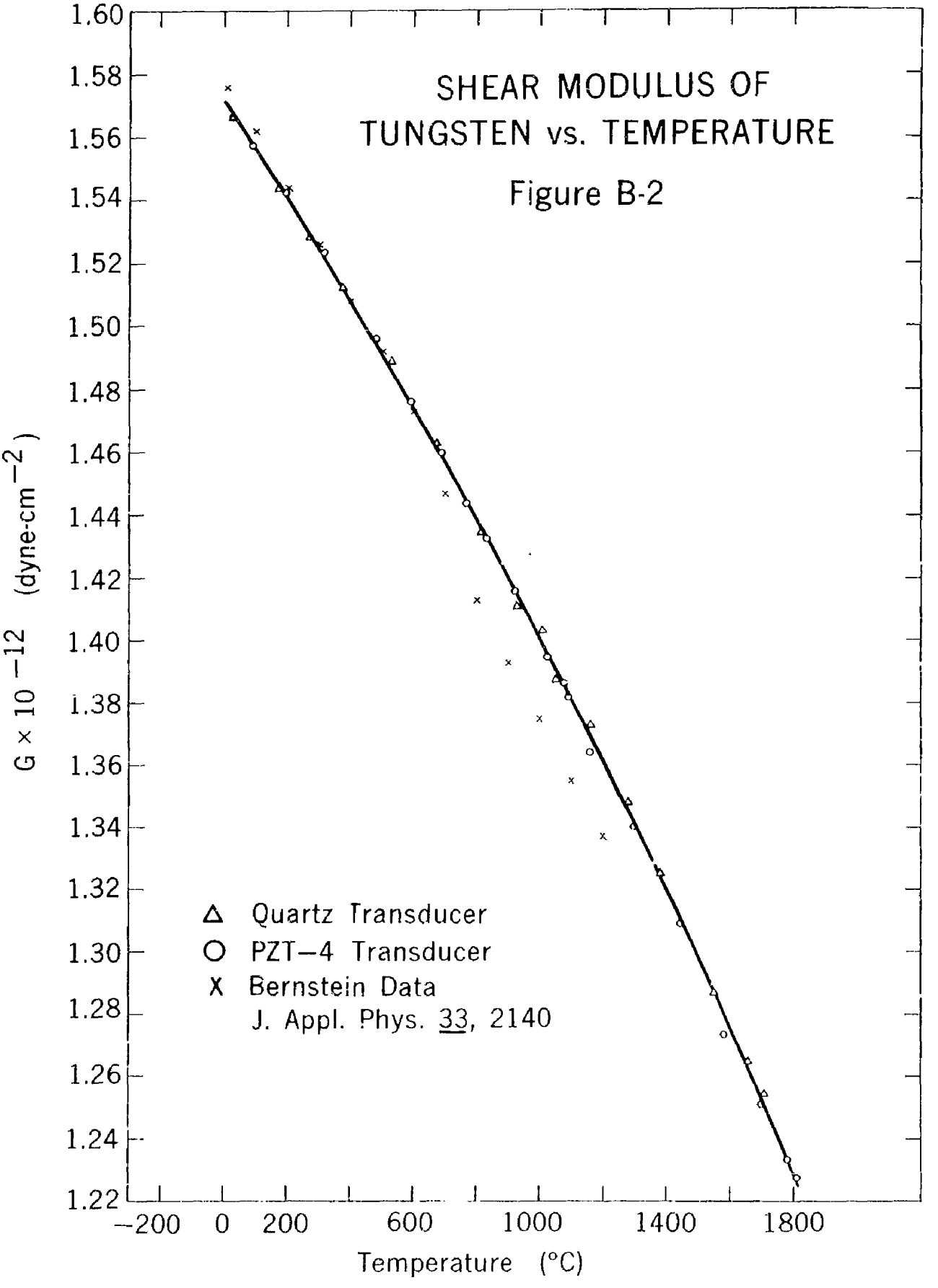
SHEAR MODULUS OF
TUNGSTEN vs. TEMPERATURE
Figure B-2
G × 10 −12 (dyne-cm −2)
1.60
1.58
1.56
1.54
1.52
1.50
1.48
1.46
1.44
1.42
1.40
1.38
1.36
1.34
1.32
1.30
1.28
1.26
1.24
1.22
−200
0
200
600
1000
1400
1800
Temperature (°C)
Δ Quartz Transducer
O PZT−4 Transducer
X Bernstein Data
J. Appl. Phys. 33, 2140

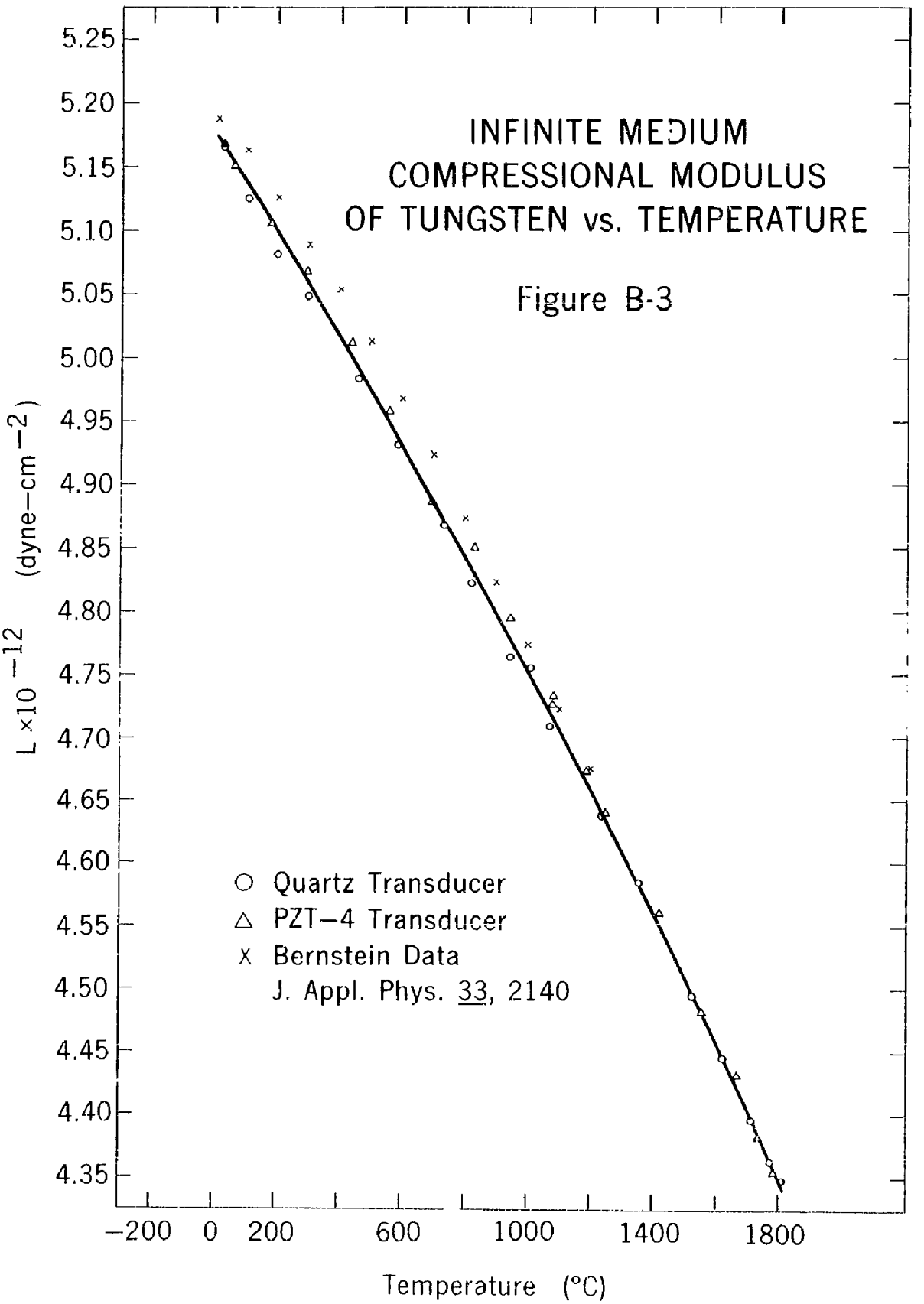
INFINITE MEDIUM
COMPRESSIONAL MODULUS
OF TUNGSTEN vs. TEMPERATURE
Figure B-3
L ×10 −12 (dyne—cm −2)
5.25
5.20
5.15
5.10
5.05
5.00
4.95
4.90
4.85
4.80
4.75
4.70
4.65
4.60
4.55
4.50
4.45
4.40
4.35
−200
0
200
600
1000
1400
1800
Temperature (°C)
○ Quartz Transducer
△ PZT—4 Transducer
X Bernstein Data
J. Appl. Phys. 33, 2140

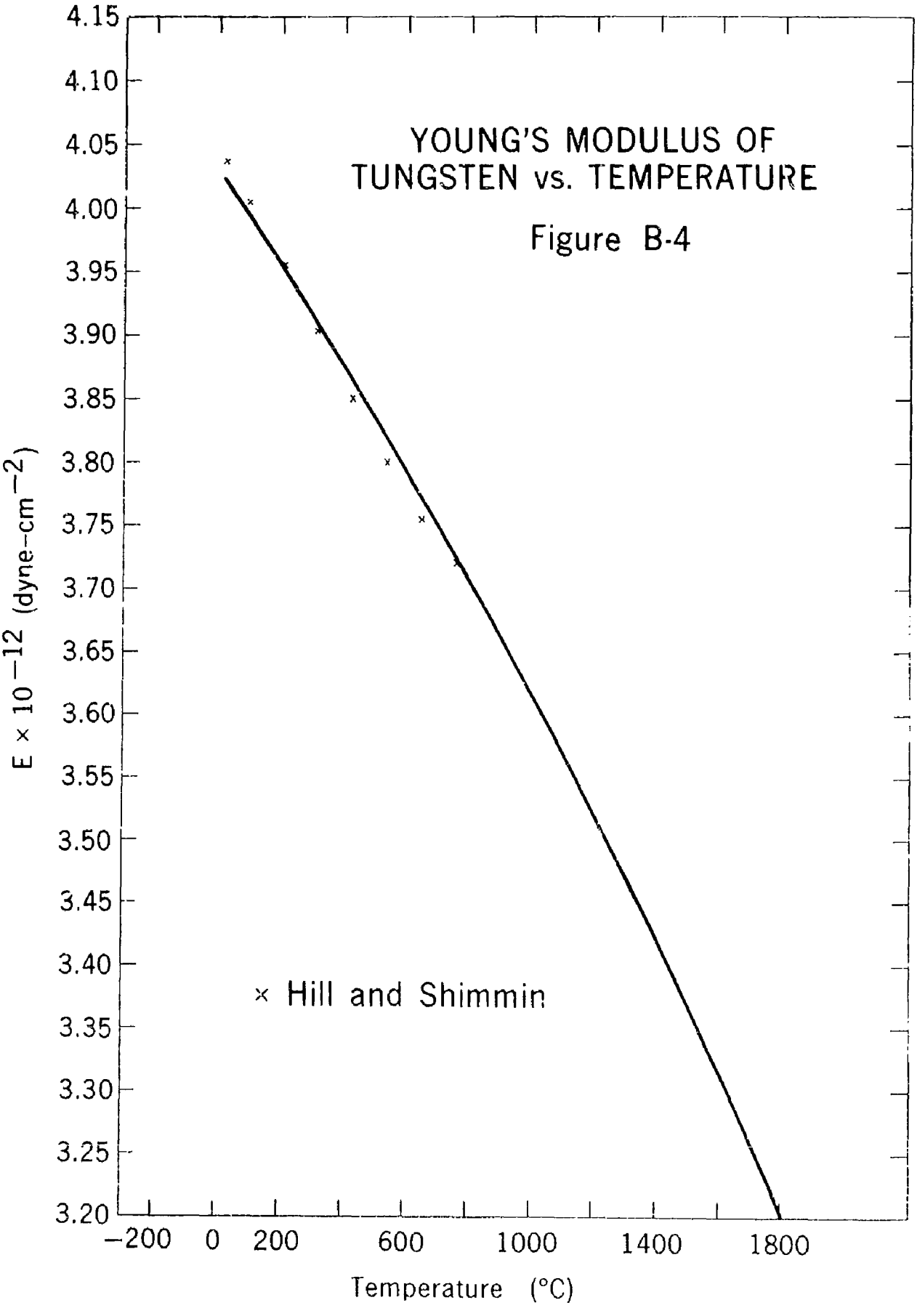
YOUNG'S MODULUS OF
TUNGSTEN vs. TEMPERATURE
Figure B-4
× Hill and Shimmin
E × 10⁻¹² (dyne-cm⁻²)
4.15
4.10
4.05
4.00
3.95
3.90
3.85
3.80
3.75
3.70
3.65
3.60
3.55
3.50
3.45
3.40
3.35
3.30
3.25
3.20
−200
0
200
600
1000
1400
1800
Temperature (°C)

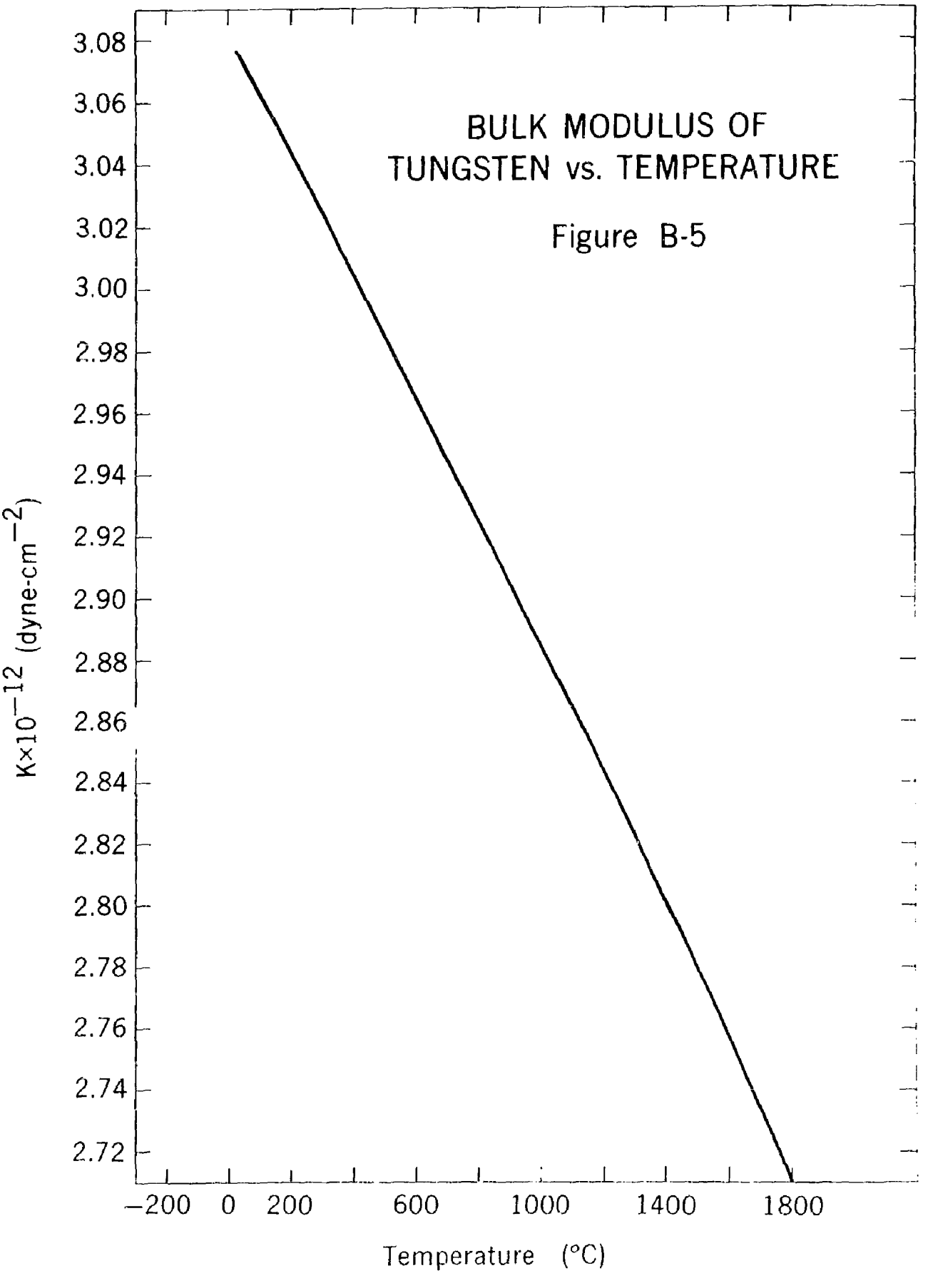
BULK MODULUS OF
TUNGSTEN vs. TEMPERATURE
Figure B-5
3.08
3.06
3.04
3.02
3.00
2.98
2.96
2.94
2.92
2.90
2.88
2.86
2.84
2.82
2.80
2.78
2.76
2.74
2.72
K×10−12 (dyne-cm−2)
−200
0
200
600
1000
1400
1800
Temperature (°C)

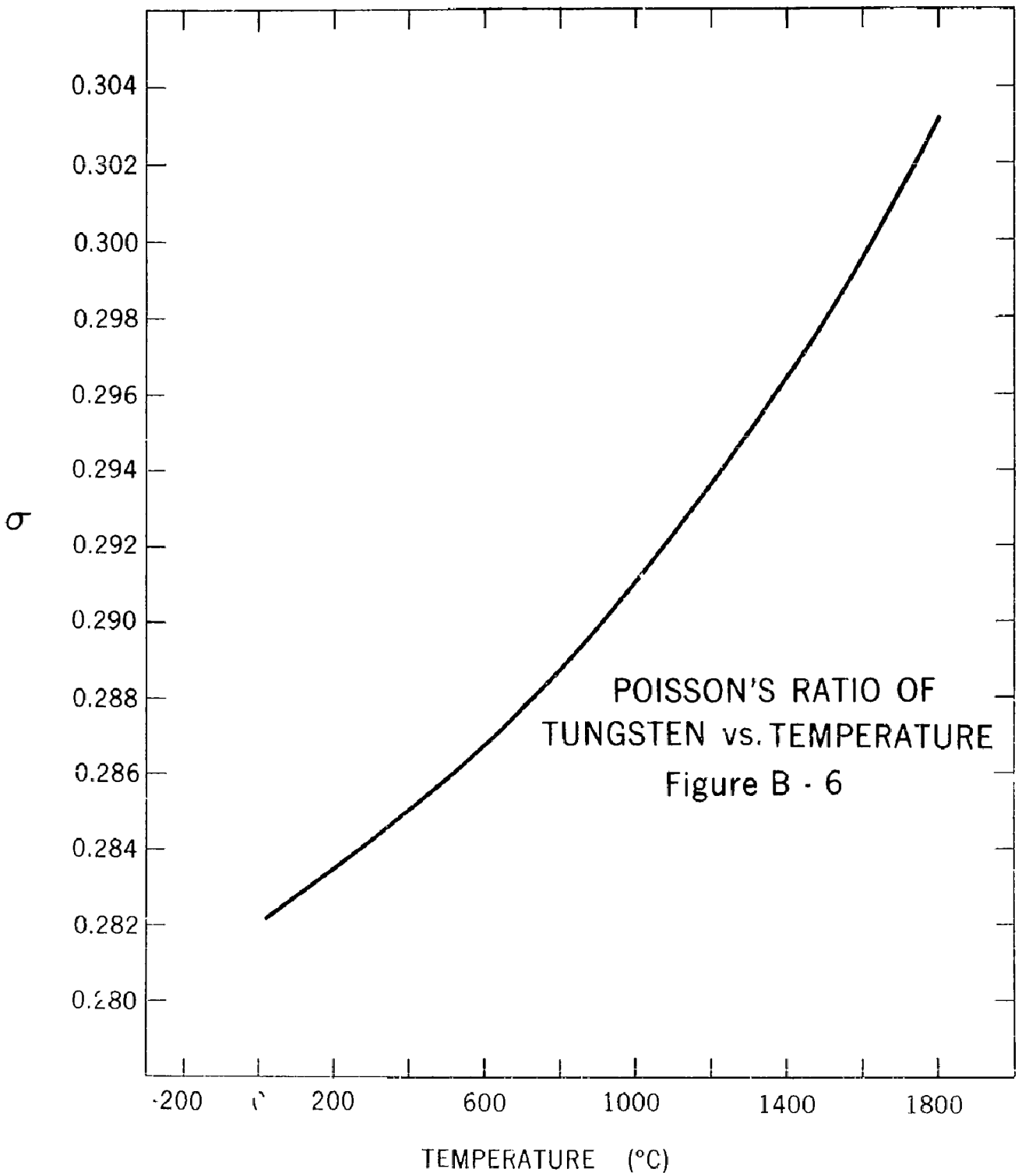
0.304
0.302
0.300
0.298
0.296
0.294
σ
0.292
0.290
0.288
0.286
0.284
0.282
0.280
-200
200
600
1000
1400
1800
TEMPERATURE (°C)
POISSON'S RATIO OF
TUNGSTEN vs. TEMPERATURE
Figure B - 6

3. High-Temperature Creep — F. G. Keihn

The high-temperature creep of three TiC specimens has been observed under different conditions of stress and temperature. Figure B-7 illustrates the rapid deformation of polycrystalline TiC at 8000 psi and 2285°K. This specimen has shown a creep rate of 8.4×10^{-5}/hr at 2200°K and 6000 psi in a previous test, in which it deformed a total of approximately 1% in 95 hours. The previous straining apparently had little effect on the creep resistance of TiC at high temperatures at higher stresses.

Clouding of the window to the total radiation pyrometer became a problem in the vacuum creep furnace after bend tests were conducted on Ni-infiltrated TaC. The test of specimen TiC-35 had to be terminated, and in the test of the specimen TiC-37 (Figure B-8) the section of the curve at 2243°K and various stresses had to be conducted using a constant power input to the furnace. A tungsten-rhenium thermocouple has since been added to the furnace as a sensing element for the controller, and the temperatures of a specimen will be read with an L & N optical pyrometer through a window which has a shutter. The shutter should prevent film formation, and the window can always be checked for film formation after the experiment.

A log-log plot for the creep rates taken from the creep curve for TiC specimen 37 (Figure B-9) indicates that this TiC has a large stress dependency for creep.

In the previous report, preliminary analyses indicated that TiC specimens No. 32 and 34 contained larger amounts of impurities than previous samples. Table B-III gives complete chemical analyses with a comparison to other TiC specimens. These large increases in the Zr and V contents might well explain the lower creep rates for specimens No. 32 and 34. Some TiC boules of higher purity have been obtained and will be tested. Unfortunately, the higher purity material always has a larger grain size, and this introduces an additional variable which influences creep rate.

Future Work. - The stress dependency will be measured on other TiC specimens, and a series of creep rates will be measured on TiC at stresses of 8000 psi and above.

Table B-III
Chemical Analyses of Creep Specimens

	TiC-25	TiC-28	TiC-32	TiC-34
Ti	79.96	80.00	79.27	79.22
C_T	19.49	19.63	19.59	19.67
C_F	.29	.31	.52	1.22
N	.14	.05	.04	.04
O	.01	.022	.030	.029
V	.004	-	.40	.43
Ag	-	.0001	-	-
Al	-	.001	.0005	.0005
As	-	-	-	-
Au	-	-	-	-
B	.001	.001	-	-
Ba	-	-	-	-
Bc	-	-	-	-
Bi	-	-	-	-
Ca	-	-	-	-
Cb	.003	-	-	-
Cd	-	-	-	-
Co	-	.003	-	-
Cr	.0006	.004	.007	.002
Cu	.002	.005	.005	.003
Fe	.093	.04	.078	.083
Ga	-	-	-	-
Ge	-	-	-	-
Hf	-	-	-	-
Hs	-	-	-	-
In	-	-	-	-
Ir	-	-	-	-
Li	-	-	-	-
Ms	.001	.0003	.0001	.0003
Mn	.007	.003	.001	.004
Mo	-	-	-	-
Na	-	-	-	-
Ni	-	-	-	-
Os	-	-	-	-
P	-	-	-	-
Pt	-	-	-	-
Pd	-	-	-	-
Pt	-	-	-	-
Rh	-	-	-	-
St	-	-	-	-
Sc	-	-	-	-
Si	.002	.0006	.001	.001
Sn	-	-	.001	-
Sr	-	-	-	-
Ta	-	-	-	-
Te	-	-	-	-
Th	-	-	-	-
Tl	-	-	-	-
U	-	-	-	-
W	-	-	.06	.06
Y	-	-	-	-
Zh	-	-	-	-
Zr	.003	.0003	.29	.31

Dash indicates element not looked for in spectrographic analysis

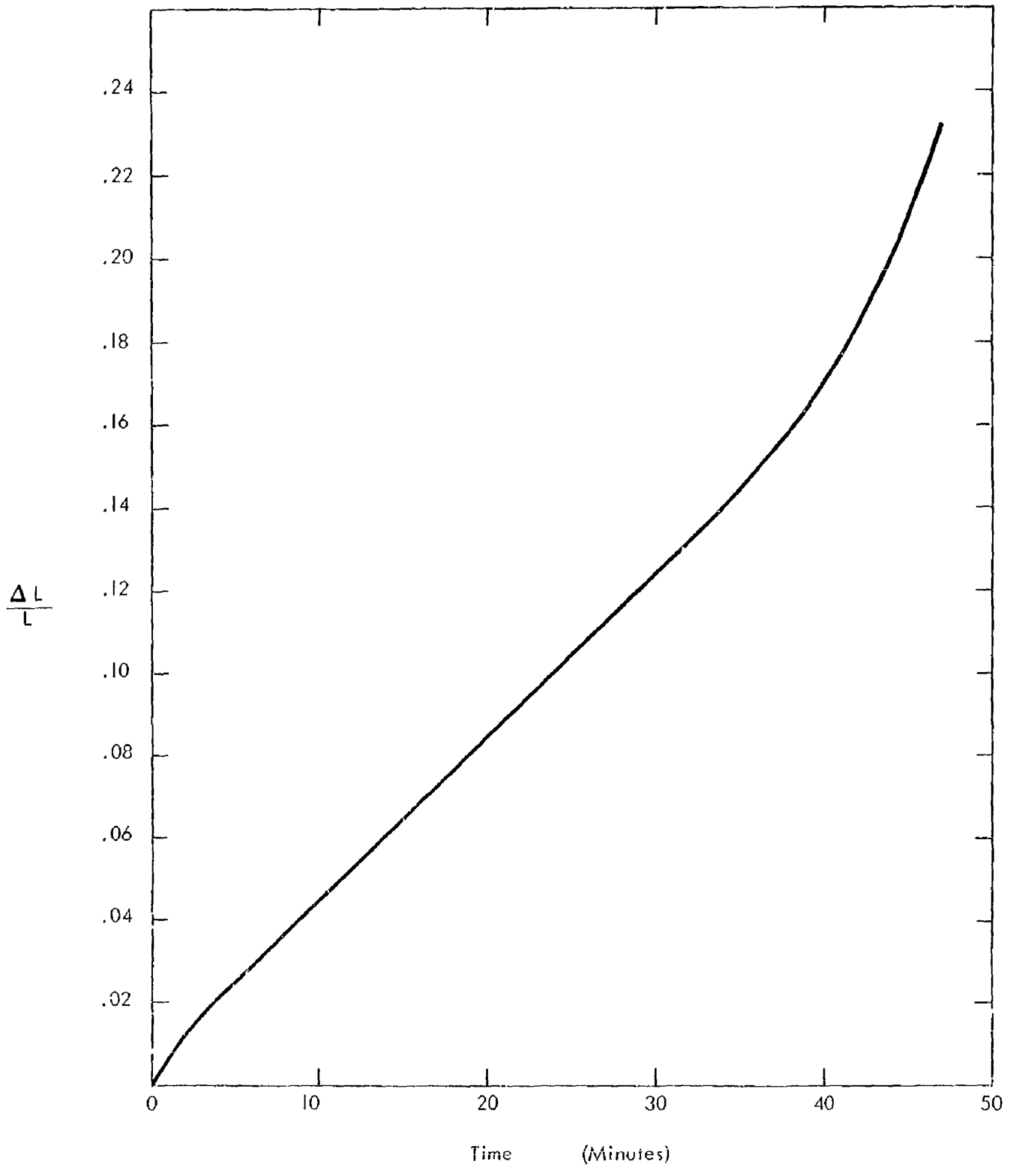

FIGURE B - 7 TiC-34 CREEP CURVE AT 2285° K AND 8000 psi

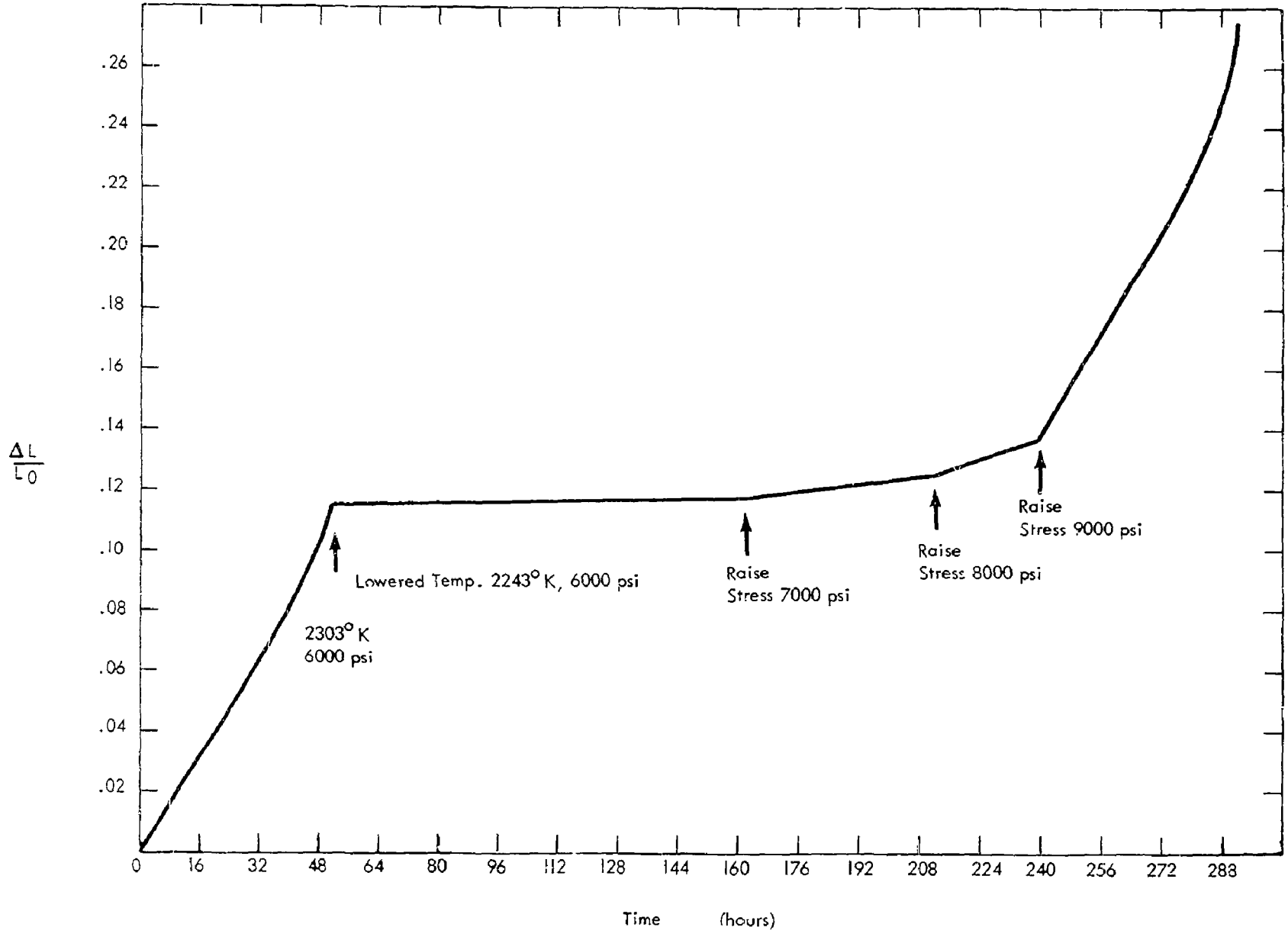

FIGURE B - 8 TiC-37 CREEP CURVE

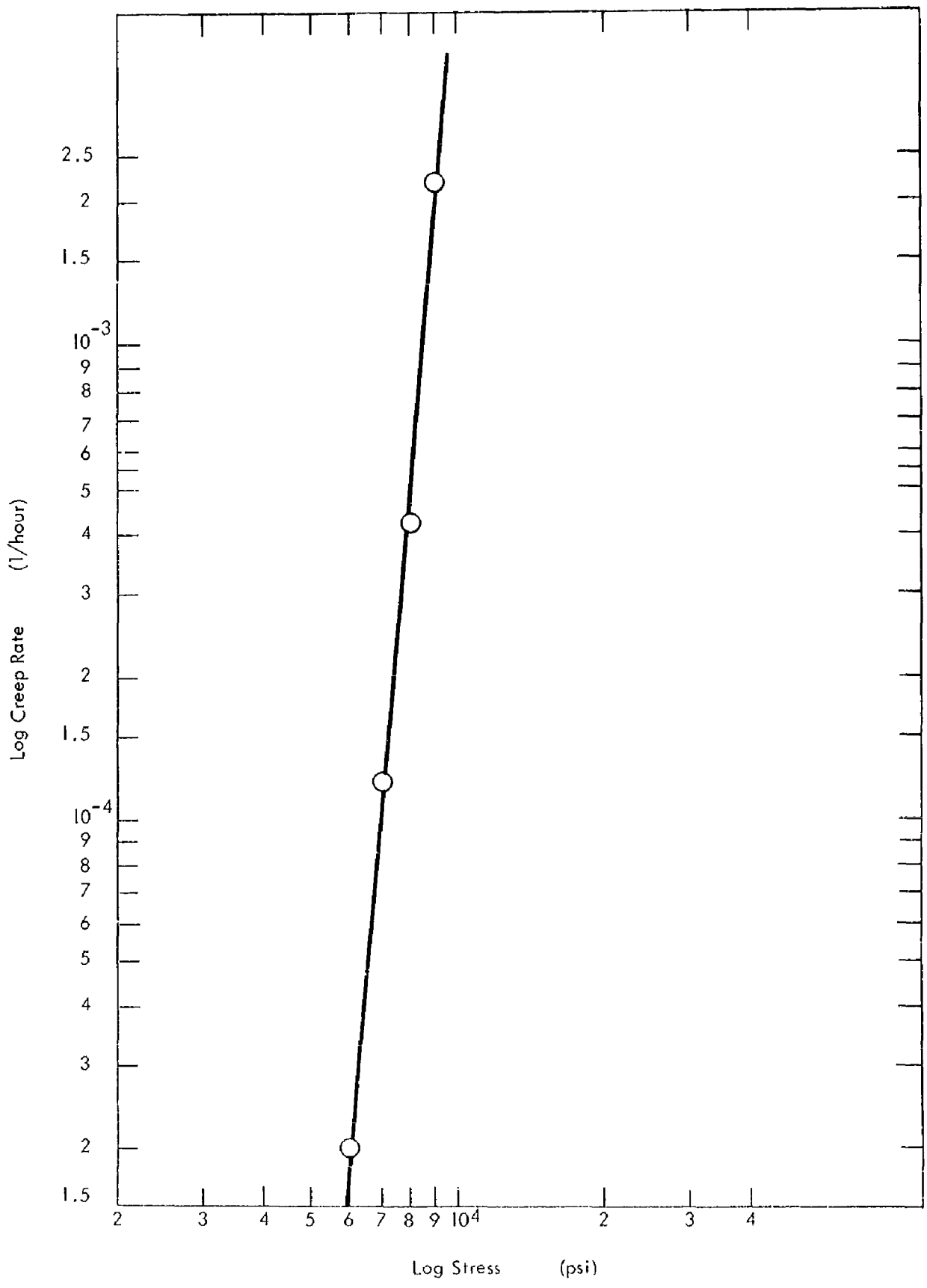

FIGURE B - 9 STRESS DEPENDENCY OF CREEP RATE OF TiC#37

4. High Temperature Creep of Refractory Metals R. L. Cummerow

Dislocations in Body-Centered Cubic Metals. - As discussed previously in QPR for June, 1964, it has been postulated by Li[1] that the rate-limiting process in high-temperature, steady-state creep is the non-conservative motion of nodes in dislocating networks. These nodes are assumed to be formed by the interaction of dislocations in a primary glide system with those in a secondary system or systems. In the body-centered cubic metals it has been found that the slip direction is invariably in the ⟨111⟩ directions, since this is the direction of closest packing and thus provides the shortest possible Burgers vector and, hence, the dislocation of lowest energy. However, there is no unique slip plane for all the body-centered cubic metals. The plane of slip varies from metal to metal and also varies with the temperature of deformation in any one metal. For niobium,[2] there is only one slip system at room temperature, $\{110\}\langle 111\rangle$, while tungsten[3] slips on both $\{110\}$ and $\{112\}$ planes at room temperature. However at higher temperatures[4] the slip systems for tungsten are found to be $\{112\}\langle 111\rangle$. Therefore, in what follows only the formation of nodes through the reaction of dislocations on $\{112\}$ planes is considered.

The application of a tensile stress is considered along the three principal crystallographic axes [100], [110], and [111] in turn. The component of force for each of the ⟨111⟩ directions is calculated for the tensile direction being considered. Then all $\{112\}$ planes with normals perpendicular to these ⟨111⟩ directions are considered. The Schmid or orientation factor, $\cos\phi \cos\lambda$, where ϕ is the angle between the axis of applied tensile stress and the slip direction and λ is the angle between the tensile axis and the slip plane normal, is then considered for each combination of 112-plane and 111-direction. The combinations with the largest Schmid factors are then taken as the active slip systems for the tensile axis considered.

---

1. J. C. M. Li, Trans. Met. Soc. AIME 227, 1474 (1963).
2. E. Votava, Phys. Stat. Sol. 5, 421 (1964).
3. H. Schadler, Trans. Met. Soc. AIME 218, 649 (1960).
4. F. S. Goucher, Phil. Mag. (6) 48, 229 (1924).

In order to make sure that the active slip systems do not change with deformation, it is necessary to consider the possible rotation of the crystallographic axes with respect to the tensile axes as deformation proceeds. In the three cases considered, the symmetry is high and the active slip directions combine to make the tensile axis the resultant slip direction. Therefore, no lattice rotation is to be expected in any of the three cases, since rotation is always in such a direction to bring the resultant slip direction and the tensile axis closer together.

The third consideration in investigating the possibility of nodal network formation is to consider the reactions of dislocations with Burgers vectors a/2 $[\bar{1}11]$ where a is the length of the cube edge. Only reactions in which the resultant dislocation has an elastic energy less than the sum of the elastic energies of the two combining dislocations are possible. For the bcc lattice the only possible reaction is:[5]

$$a/2\ [111] + a/2\ [1\bar{1}\bar{1}] = a\ [100].$$

Since the elastic energy of a dislocation is proportional to the square of its Burgers vector, the elastic energy of the resultant dislocation is smaller by an amount proportional to $a^2/2$.

The following table summarizes the results of these considerations for the axis of tension in the three principal crystallographic directions.

Tensile axis	Slip Systems	Schmid Factor	Nodal Network Formed
[100]	$(2\bar{1}\bar{1})$ [111] (211) $[\bar{1}\bar{1}\bar{1}]$ $(2\bar{1}1)$ $[11\bar{1}]$ $(21\bar{1})$ $[1\bar{1}1]$	0.47	yes
[110]	$(\bar{1}\bar{1}2)$ [111] (112) $[\bar{1}\bar{1}\bar{1}]$	0.47	no
$[11\bar{1}]$	$(2\bar{1}\bar{1})$ $[\bar{1}1\bar{1}]$ $(\bar{1}\bar{1}2)$ $[\bar{1}11]$ $(1\bar{2}\bar{1})$ $[1\bar{1}\bar{1}]$	0.44	no

---

5. Amelinckx and Dekeyser, Solid State Physics, [illegible], Volume 8, Academic Press, [illegible].

Thus, only with the axis of tension in the [100] direction would a nodal network of the type postulated by Li[1] be formed. The rate-limiting step for steady-state creep in the [100] direction might be expected to be the diffusive motion of nodal [100] segments postulated by Li. The activation energy would be close to that for self diffusion. The creep strain rate would be expected to be proportional to the applied stress to the power n, where according to Li's theory n is equal to the number of atoms in the nodal [100] segment. In the other two crystallographic directions, based upon the collective experience with steady-state creep, the basic rate-limiting step would again be self-diffusion, but the diffusing entity would not be expected to be a nodal dislocation segment. It might be, for example the diffusive motion of prismatic dislocation loops interacting with glide dislocations. Therefore, for these two directions for a given temperature, the value of n would be expected to be different from that for the [100] direction, even though the activation energy would be the same.

Important information about the dislocation mechanisms active in steady-state creep may be gained by studying this phenomenon as a function of the crystallographic orientation of high-purity crystals, both macroscopically and electron-microscopically.

Apparatus. The electron-beam zone refiner is being used to refine 1/4 inch tungsten rod. The addition to the bell-jar chamber of a Varian titanium getter pump has improved the working vacuum from the 10^{-6} to 10^{-7} torr range. This pump greatly facilitates starting the Vac-ion pump after pump-down by means of the liquid-nitrogen sorption pump.

The diameter of zone refined specimens has not been sufficiently uniform so that they can be used for tensile specimens. It is believed that this uniformity can be achieved by electronically controlling the current as has been done by Votava[6] and others. A commercial power supply with control features which can be adapted for this purpose is being considered.

If production of samples for tensile creep experiments by this zone refiner is delayed, materials will be procured from other sources for the first experiments.

---

6. E. Votava, private communication.

The development of methods for electrolytic shaping of samples for the creep experiments is proceeding satisfactorily using standard electrolytic polishing and etching techniques in combination with the application of stop-off laquer. An automatic arrangement for turning the sample end-for-end has been constructed. By using these techniques it is possible to produce a sample with cylindrical knobs on each end with a gauge section in the middle. These methods will also be extended to produce thin, oriented sections for electron microscopy.

The construction and testing of the high-vacuum tensile tester is proceeding in parallel with these other preparations. The heater, heat shields, and sample holders have been completed, and the chamber is being vacuum-checked before testing of the heater, power supply, and temperature control circuits.

C. Specimen Preparation and Characterization

1. Purification and Sample Preparation — I. Binder

Small amounts of pure Nb-B and Ta-B compositions have been prepared for x-ray study. An NbB_2 specimen has been heated in the vacuum furnace under various conditions to investigate its stability in vacuum at high temperature. When NbB_2 is heated in high vacuum for several hours at 1500°C, boron seems to be lost from the surface.

A second set of TiC specimens was hot pressed for strength and heat-treatment studies (QPR, June 1964). The zone-refining setup was used to make a sound joint between a machined tungsten single crystal and its long polycrystalline tungsten support rod in order to make acoustical measurements of elastic constants.

Most of the specimen preparation work this quarter has been on composite materials and is discussed in Section D-1.

2. Analytical Research — G.J. McKinley, H.F. Wendt

a. Determination of Boron. A determination of boron in refractory borides by pyrohydrolysis and titration of the boron oxides thus produced would be attractively simple to perform. In this respect, it would be preferable to the current peroxide fusion method, which has many more steps and requires constant attention. Last quarter, we described a few pyrohydrolysis experiments run by passing steam over the heated sample in an apparatus consisting of a steam generator, a Vycor reaction tube, and a condenser with a dip tube into the receiver flask. The rate of pyrohydrolysis of zirconium diboride was reasonably fast at 900°C, and boric acid recovery was complete in about three hours. This quarter, attempts were made to improve upon these results by (1) adding oxygen to the steam and (2) carrying out the reaction at higher temperatures.

Since the boron in refractory borides becomes oxidized in the pyrohydrolysis reaction, it was thought that adding oxygen might speed up the reaction. In order to test this, runs were made at 600°, 700°, 800°, and 900°C while adding oxygen through a bubbler in the steam generator at a

rate of one and one-half times the stoichiometric requirement per minute. Titrations of the boric acid in the distillate were made at one-hour intervals during these runs. No improvement in reaction rate was observed over that measured for runs without added oxygen.

The use of higher temperatures to shorten the analysis was tried out on zirconium diboride, at 1100°C and 1200°C. Because of the higher temperatures, a nickel combustion tube was substituted for the Vycor tube. Spectrographic analyses of the residues obtained from a one-hour run at 1100°C and a thirty-minute run at 1200°C indicated that all but a trace of the boron had been evolved. However, the titrations of the blank determinations at the two temperatures were abnormally large, and titrations of the distillates yielded boron values higher than expected. Examination of both distillates revealed the presence of nickel, which apparently came over with the boron in the distillation process and interfered with the titration. It appears that a special step to remove the nickel would be necessary, but this would destroy the attractive simplicity of the method. Consequently, a quartz combustion tube was tried in one-hour pyrohydrolyses of six samples of the ZrB_2 and eight samples of TiB_2 at 1100°C (considered to be the maximum safe operating temperature for quartz). The results (Table C-I) indicates a complete recovery of boron, agreeing well with the routine peroxide fusions previously made but seemingly being somewhat more precise.

Quantitative spectrographic analyses of the residues from the pyrohydrolysis runs listed in Table C-I indicated a residual boron content of less than 0.02%, which is equivalent to less than two parts per thousand of the boron present in the original sample. Examination of these same residues by x-ray diffraction proved them to be rutile (TiO_2) in the titanium diboride series and baddeleyite (ZrO_2) in the zirconium diboride series.

In order to make a preliminary evaluation of the application of the pyrohydrolysis technique to borides other than those of titanium or zirconium, several laboratory control samples which had previously been analyzed by the peroxide fusion procedure were subjected to pyrohydrolysis at 1100°C. These samples were available only in small quantities and therefore only single determinations were run on each. The zirconium diboride and titanium diboride

TABLE C-I

PRECISION DATA FOR BORON RECOVERY (in % Boron)

	Pyrohydrolysis Method		Routine Peroxide Fusion Method	
	ZrB_2	TiB_2	ZrB_2	TiB_2
	18.74	30.97	18.61	31.07
	18.79	30.98	18.67	30.84
	18.78	30.89	18.70	30.83
	18.76	30.95	18.69	30.72
	18.70	30.92	18.63	31.32
	18.74	30.81	18.63	31.18
		30.86		
		30.82		
Mean	18.75	30.90	18.66	31.00
Std. Deviation	0.03	0.07	0.04	0.23

samples were powders of less than 200 mesh in size. The mesh size of these other borides was unknown, but visual examination indicated particle sizes probably greater than 200 mesh. The data obtained (Table C-II) suggested that additional work will be required to determine the proper experimental conditions for pyrohydrolysis of some of these other borides. Moreover, since the rate of pyrohydrolysis may be a function of particle size of the sample, it will be necessary to use powders of comparable size (i.e. 200 mesh) to evaluate the effectiveness of the procedure when applied to these other borides.

TABLE C-II

BORON RECOVERY FROM METAL BORIDES

Sample	% Boron By Pyrohydrolysis At 1100°C	% Boron By Peroxide Fusion Procedure	Notes
HfB_2	6.8	10.42	Recovery incomplete after four hours
TaB_2	10.5	10.53	Recovery complete in one hour
NbB_2	17.8	18.16	Recovery complete in one hour
LaB_6	29.8	34.28	Pt boat severely etched. Fused B_2O_3 found in boat.
YB_6	29.5	37.57	Recovery incomplete after two hours
YbB_6	27.0	29.52	Recovery incomplete after two hours
CrB	16.7	17.18	Recovery incomplete after two hours

A further refinement in the titration of the evolved boric acid by the procedure with mannitol and sodium hydroxide has been attempted. This procedure normally consists of (1) the neutralization of the free mineral acid in the sample to be titrated, (2) the addition of mannitol to transform the boric acid into a relatively strong complex acid, and (3) the titration of the complex acid with a standard solution of sodium hydroxide. The success of this procedure is therefore dependent on the careful selection of two end points, the point at which the mineral acid is neutralized and the point at which the mannitol complex is neutralized.

References in the literature to the selection of these end points are many and varied. Some authors recommend the use of visual indicators. Those who recommend potentiometric titration seldom indicate the means by which

the points have been determined. This uncertainty becomes a pertinent problem in the analysis for boron by pyrohydrolysis since the final result is obtained by titration of the boric acid evolved. However, one attractive feature of the pyrohydrolysis method is the fact that this titration is always made on a pure solution of boric acid, free of contaminating ions, and varying only in boric acid concentration. The problem then becomes simply one of determining the best end points for pure boric acid solutions of various concentrations.

In order to select the two end points, four solutions of known amounts of reagent-grade boric acid were titrated, and the potentiometric titration curves were plotted for each one. From these data the two end points were calculated using the second derivative method of Lingane.[1] The average values were pH 5.64 for the first end point and pH 8.00 for the second end point. With these values the amount of boron in a known boric acid solution was determined as 17.51% in excellent agreement with the known value of 17.48%.

b. Future Work. During the next quarter pyrohydrolysis will be attempted on -200 mesh samples of niobium diboride, tantalum diboride, and hafnium diboride. At the conclusion of this work our efforts will be directed to a study of the caustic fusion technique for the determination of nitrogen as applied to borides, carbides, and nitrides. A research report describing the pyrohydrolysis method for boron is now in preparation. Later, the work on the free carbon determination will be reviewed, and a compilation of the methods used by this laboratory for the analysis of the borides, carbides, and nitrides will be prepared.

---

1. Lingane, J. J., Electroanalytical Chemistry, [illegible], 2nd Ed., Interscience, New York (1[illegible]).

D. Composites

1. Material Preparation I. Binder

The preparation of composite materials, consisting of porous hardmetal bodies infiltrated with metal, was continued with TaC as the primary high-temperature skeletal material. This work included preparation of large batches of hardmetal powders so that many specimens could be made from the same starting materials, hot pressing of hardmetal skeletons, development of uniformity in the infiltration process, and a start on isostatic pressing as a means of producing uniformly porous hardmetal bodies.

a. Specimens for Mechanical Testing. A large number of test bars of TaC, TaC + Ag, and TaC + Ni were prepared for mechanical testing and for gas reaction studies. All the test bars, both plain TaC and infiltrated, were ground with a resin-bonded diamond wheel, to give size uniformity and to remove surface imperfections.

The usable high-temperature strength of a composite body will be determined by the strength of the high-melting skeleton. Since the strength of a specimen is a function of its density, higher density TaC bodies than those normally used for infiltration blanks were prepared for strength tests to determine this dependence. Using the same coarse powders as those used for the composite skeletons, a maximum of approximately 90 percent of theoretical density was attained, as compared with the 75 to 84% density in bars used for infiltration. Still higher densities can be obtained by using powders ball milled to finer sizes, but these powders will contain larger amounts of impurities. The powders used for the infiltrated composites were screened to -270 mesh and averaged 6.4 microns on a Fisher SubSieve Sizer.

The gas-solid reactions will be conducted on 3/16" square pieces cut from the fractured room-temperature impact bars. This testing is being done because the specimens now prepared are much more uniformly infiltrated with nickel than were those previously tested, and improved behavior is expected.

b. Improved Infiltration Method. An improved procedure has been developed for infiltrating carbide blanks with nickel. Originally, the infiltration was done in the hot press at temperatures over 1900°C (the external surface of the graphite die read 1740°-1770°C with a radiation pyrometer). This process involved very rapid heating and a considerable solution of the carbide in the nickel, and it generally produced severe pitting.

Nickel infiltration of hot-pressed TaC compacts in a tube furnace has produced much more uniform specimens. While the time and temperature of infiltration have not been optimized, TaC bars, 75 to 84% dense and containing essentially continuous fine porosity, have been successfully infiltrated with nickel at 1470°C in an argon atmosphere. There is no pitting or gross porosity, although there is visual evidence of a thin layer of surface reaction with the nickel. The metal is well distributed throughout the bar, and metallographic examination shows 95 to 100 percent of the pores to be metal-filled. Assuming all the weight gain to be nickel pickup, the densities of the infiltrated bars also correspond to 95 to 100 percent of that expected for the addition of 10 percent nickel by weight.

In general, the nickel-infiltrated TaC composites appear to be mechanically sound and with dimensions as uniform as the blanks from which they are prepared. Only one such bar showed a flaw - this sample was warped, probably because of a large variation in density along the length of the original hot-pressed bar.

Similar infiltration experiments in tube furnaces with silver as the infiltrant have been less consistent. Silver does not wet the carbide grains well and has too great a viscosity to flow at temperatures just over its melting point. This agrees with hot press infiltration tests with silver, in which temperatures well over 1900°C, applied for very short times, were required for adequate filling of the pore skeleton. At furnace temperatures of 1450°C, silver flowed into the pores of carbide compacts, but it also vaporized to a considerable degree, due to the much longer times required for heating and cooling. This led to irregular distribution of infiltrant in these pieces, with correspondingly inconsistent properties. Since only a few such tests have been made, it is quite possible that an intermediate temperature can be found at which silver infiltration will proceed smoothly and uniformly. However, it appears more likely that a metal such as silver

will be infiltrated best by a more rapid heating process, either in a die in a hot press or, more economically, by high-frequency heating in a controlled atmosphere furnace.

c. Other Hardmetals. Furnace infiltrations of nickel into hardmetals other than TaC have been tried. In each case, a hot-pressed skeleton, 75-85 percent dense, was the starting material. Some ZrB_2 bars infiltrated properly, although this material is more difficult to form into a uniform compact with continuous fine porosity. A ZrC bar from a batch much less pure than the TaC currently in use was partly infiltrated, to the point at which the bar split apart on a pressing lamination. A NbB_2 specimen stuck badly to the graphite die and broke into several pieces. Hot-pressed bars of NbC, TiB_2, TaB_2, YbB_6, ZrN, and TiN have also been prepared for future infiltration.

d. Isostatic Pressing. A different approach to composite formation has been started, not using the hot press to fabricate the porous blanks for infiltration but forming them by cold isostatic pressing, followed either by direct infiltration or by a partial sintering and then infiltration. Isostatic pressing has the advantage of producing uniform, reproducible compacts without the use of very high temperatures, and it is also an economically feasible means of fabrication. In addition, isostatic presses are not subject to the inherent size limitations of a fast-acting hot press. However, the densities attainable are lower than in hot pressing, generally requiring an intermediate sintering step prior to infiltration.

A 60,000 psi isostatic press with a pressure chamber 3" in diameter and 18" high has been obtained from the National Forge Company. In this equipment, in which a simple piston pump is operated by tank gas to develop pressure, ZrC and NbC cylindrical compacts have been pressed, using a small amount of camphor as a fugitive binder and lubricant. The resulting specimens were 50-65% dense, uniform in appearance, and strong enough to be cut with a hacksaw. One ZrC cylinder and half a NbC cylinder were sintered in a tube furnace as a preparation for infiltration. The other half of the NbC was used directly for nickel infiltration. This was done to determine whether the porosity developed by isostatic pressing could be infiltrated well. Visual inspection of this NbC indicates that it was very well infiltrated by a large (25 volume %) of nickel.

The particle size of the powder is important both for the degree of densification achieved in isostatic pressing and for the green strength of the pressed sample. With NbC of average size 15 microns (measured on the Fisher SubSieve Sizer), the compact was too loose and powdery to be used, but sizes of 6 to 8 microns yielded solid bars that could be handled for further processing.

There is still a great deal to be learned about the optimum conditions of isostatic pressing: particle size and size distribution of the hardmetal powder; amount and composition of the fugitive binder; operating pressure; time to achieve this pressure; dwell time; design and composition of the mold to facilitate stripping and prevent sticking and tearing of the compact.

Future work will include heating isostatically-pressed rods in the zone-sintering furnace to achieve rapidly the densities required for proper infiltration and to develop sufficient strength in the high-melting hardmetal skeleton. In addition, this procedure could lend itself to the formation of a structure with a graded density, into which varying amounts of metal could be infiltrated.

e. ZrC. A large lot of ZrC is being assembled for composite work. This is being prepared in several smaller batches, each of which is being vacuum purified and chemically analyzed before addition to form one batch. This detailed check on consistency is more necessary with ZrC than with TaC, since the level of impurities in ZrC is higher. While the exact effects of impurities are not yet known, infiltration is more successful and more uniform with base materials of the highest purity.

f. Future Work. Hardmetal composites, isostatic pressing for infiltration blanks and for zone sintering, better control of the infiltration procedure, and physical property measurements of machined composite specimens will be emphasized during the next quarter.

2. Mechanical Properties of Infiltrated TaC — F. G. Keihn

Some transverse rupture strengths of TaC and infiltrated TaC have already been reported (QPR, December 1963 and March 1964). The data were collected using a carburized TaC (three point) fixture within the vacuum creep furnace. Because of the loss of Ni in the vacuum furnace, a carbon tube furnace with argon atmosphere has been set up. A Honeywell controller with a tungsten rhenium thermocouple as the temperature sensing element is used to control this furnace.

A 20-to-1 lever with hardened-steel knife edges was arranged on the top of the furnace to load the sample through a water-cooled "O" ring. The load was applied by adding shot to a bucket at the end of the lever. The load applied by the lever system was checked by replacing the sample with dead-weight loading. A maximum error of 5% because of the "O" ring friction and misalignment was found. As a further check, a sample of TaC was dead loaded outside the furnace in transverse rupture fixtures. Previous transverse rupture strengths on a Dillon testing machine averaged 43,000 psi at room temperature where the density of the specimens was slightly higher — 13 g/cc as compared to 12 to 12.5 for the present samples, which were all hot-pressed bars .050" x .200" x .750".

The data are summarized in Figure D-1. Because of the variation in hot-pressed TaC from sample to sample, rather wide limits should be placed on any individual value of strength. Nonetheless, the data clearly indicate a minimum in the transverse rupture strength of hot-pressed TaC around 1400°C. Further studies will be made of this minimum, which would appear to be a consequence of the occurrence of some plastic deformation above 1400°C.

The strength of Ni-infiltrated TaC was maintained well to about 900°C and then rapidly decreased until the bars broke before they could be loaded at 1400°C. This is reasonable since the Ni with TaC in solution probably melts about 1400°C and dissolves most of the TaC-TaC bonds previously formed during hot pressing. It was observed also on sandwiches consisting of TaC-Ni with tungsten, tantalum, and TaC that the Ni migrated from the composite to the tungsten, tantalum, or TaC at approximately [illegible] °C.

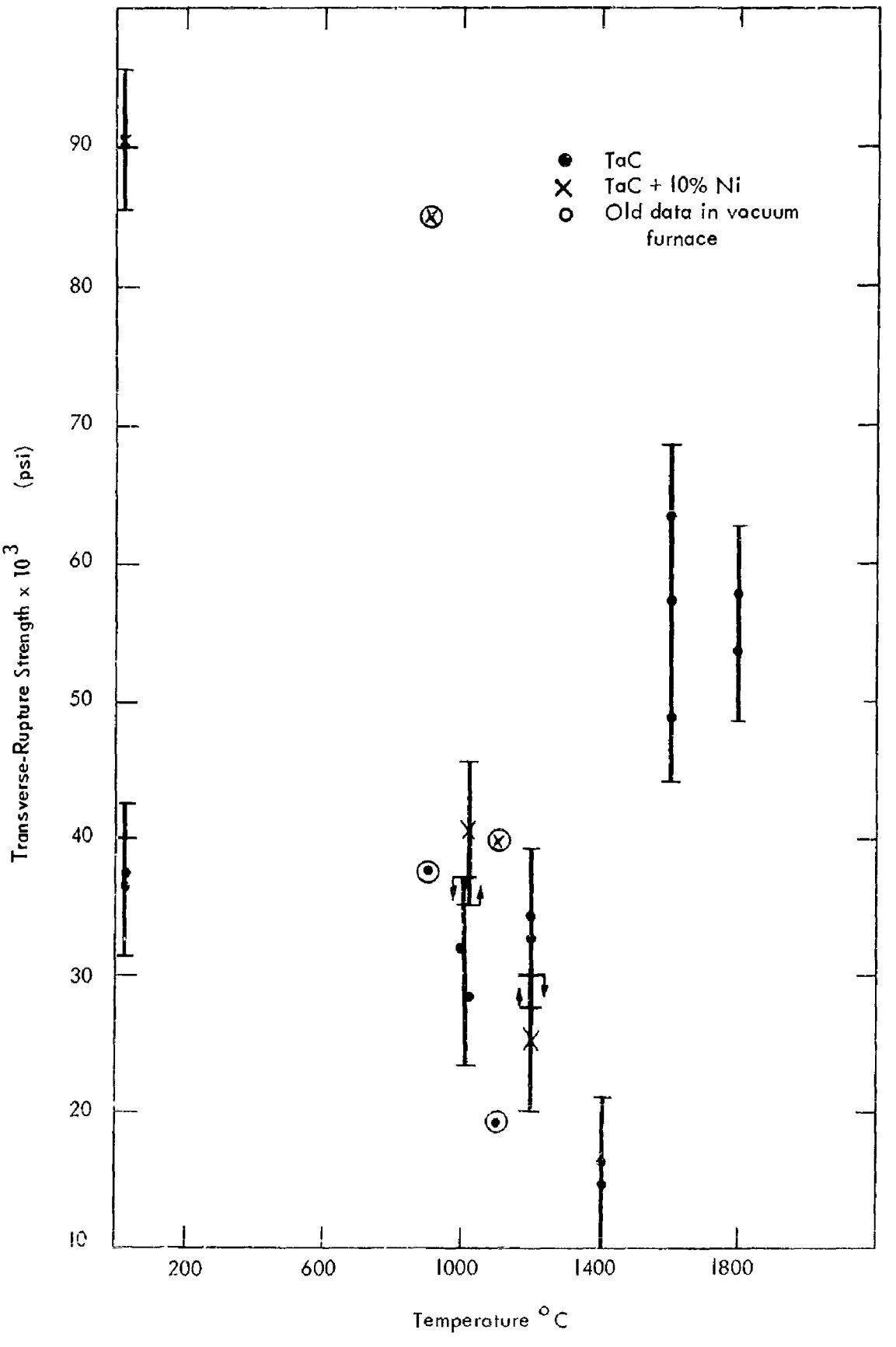

FIGURE D - 1 TRANSVERSE-RUPTURE STRENGTHS OF TaC AND TaC + 10% Ni

A group of TaC and Ni-infiltrated TaC bars were taken to Alfred University and broken on a Tinius Olsen testing machine for microcharpy impact strengths. All bars were approximately 1 3/8" x 3/16" x 3/16". A standard 50 in. lb. head was used with a 1 1/4" gap. The impact strengths are listed in Table D-I with typical impact strengths for other materials. It can be seen that the strengths compare favorably with other conventionally prepared carbides.

Table D-I

Microcharpy Impact Strength of Cermets

(unnotched specimens 3/16" square)

Material	Impact Strength (in. - lb.)	Reference
TaC	0.5 - 1.0	Our data
Ni-infiltrated TaC	1.75 - 2.5	" "
Ni-cemented Ti(CbTa)C	4.1 - 5.1	(1)
Ni-Mo-cemented Ti(CbTa)C	1.5 - 2.8	(1)
Ni-cemented Ti(Cr)C	1.8 - 3.0	(1)
Superalloy X-40	40-50	(1)

(1) J. Wambold, "Carbide-Base Cermets", pp. 140 in Cermets, edited by J. R. Tinklepaugh and W. B. Crandall, (1960) Reinhold Publishing Corp.

IV RECENT PUBLICATIONS AND PRESENTATIONS

Presentations

"Nozzle-Wall Chemical Corrosion", R. W. Kebler and R. A. Graff, presented at the Nozzle Heat Transfer and Erosion Meeting sponsored by the Solid Rocket Division of the Air Force Rocket Propulsion Laboratory, Edwards Air Force Base, California, September 1, 1964.

"Kinetics of the Oxidation of Tungsten by CO_2 above 2000°K," I. R. Ladd, J. M. Quets, J. E. Smith, R. A. Graff, and P. N. Walsh. Presented at the Symposium on High-Temperature Chemistry of the Chemical Institute of Canada, September 2-4, 1964 in Ottawa, Ontario.

Research Reports

"Thermal Expansion and Atomic Vibration Amplitudes of TiC, TiN, ZrC, ZrN, and pure Tungsten", C. R. Houska, Research Report C-17, August 1963.

"High Temperature Thermal Expansion of Certain Group IV and V Carbides", C. R. Houska, Research Report C-18, December 1963.

"The Reaction of Active Nitrogen with Graphite", H. W. Goldstein, Research Report C-19, December 1963.

"Bibliography on Analytical Chemistry Relating to Borides, Carbides, and Nitrides of Group IV and V Elements", M. R. Bateman, G. J. McKinley, G. H. Clewett, and H. F. Wendt, Research Report C-20, December 1963.

"Electrical Properties of Some Transition-Metal Carbides and Nitrides", John Piper, Research Report C-21, April 1964.

"Static Atomic Displacements Resulting From Vacancies in Defect Structures $TiN_x\square_{1-x}$", C. R. Houska, Research Report C-22, April 1964.

Publications

"The Reaction of Active Nitrogen With Graphite", H. W. Goldstein, J. Phys. Chem. 68, 39-42 (Jan. 1964).

"High-Temperature Furnace for Quantitative X-Ray Intensity Measurements", C. R. Houska and E. J. Koplin, J. Sci. Inst. 41, 23-27 (Jan. 1964).

Publications (Cont'd.)

"Thermal Expansion and Atomic Vibration Amplitudes for TiC, TiN, ZrC, ZrN, and Pure Tungsten", J. Phys. Chem. Solids 25, 359-366 (April 1964).

"Thermal Expansion of Certain Group IV and Group V Carbides at High Temperatures", C. R. Houska, J. Am. Cer. Soc. 47, 310-311 (June 1964).

"High-Temperature Ductility of Large-Grained TiC", F. G. Keihn and R. W. Kebler, J. Less Common Metals 6, 484 (June 1964).

DISTRIBUTION

Advanced Research Projects Agency (5)
Washington 25, D. C.
Atn: Mr. T. O. Dobbins
Advanced Propellants Chemistry
Office

National Academy of Sciences
Washington, D. C.
Atn: Dr. Guy Waddington

National Aeronautics & Space Admin.
Washington 25, D. C.
Atn: Office of Technical Information
& Educational Programs
CODE ETL

Atn: CODE MEG, Miss Carol Funk

Scientific & Technical Information
Facility (2)
Bethesda, Maryland
Atn: NASA Representative

National Aeronautics & Space Admin.
Lewis Research Center
Cleveland 35, Ohio
Atn: Library

National Aeronautics & Space Admin. (3)
Langley Research Center
Langley Air Force Base, Virginia
Atn: Library

National Aeronautics & Space Admin.
Goddard Space Flight Center
Greenbelt, Maryland
Atn: Library

National Aeronautics & Space Admin.
George C. Marshall Space Flight Center
Huntsville, Alabama
Atn: Library

National Aeronautics & Space Admin.
Manned Spacecraft Center
Houston 1, Texas
Atn: Library

National Bureau of Standards
Washington 25, D. C.
Atn: Dr. S. Madorskey

Atn: Dr. Charles W. Beckett, Jr.,
Chief (2)
Thermodynamic Section
Division of Heat & Power

Oregon Metallurgical Corporation
Albany, Oregon
Atn: Mr. Russell G. Hardy

U. S. Atomic Energy Commission
Office of Technical Information Ext.
Oak Ridge, Tennessee

U. S. Dept. of Interior
Bureau of Mines
Pittsburgh 13, Penn.
Atn: M.M. Dolinar, Reports Lib.
Explosives Res. Laboratory

U. S. Bureau of Mines
Petroleum Research Center
Bartlesville, Oklahoma
Atn: Dr. John P. McCullough

Institute for Defense Analysis
Research & Engineering Support Div.
Washington 9, D. C.
Atn: Technical Information Office

U.S. Army Missile Command (5)
Redstone Arsenal, Alabama
Atn: Redstone Scientific Information
Center

Atn: AMSMI-IXDA

Atn: AMSMI-RRP

Atn: AMSMI-IXD

Atn: AMSMI-RFE (8)

Atn: AMSMI-RK (Mr. B.J. Alley)

New York Procurement District
New York 3, New York
Atn: AMSMI-OBM

Chief, New York District
U. S. Army
New York 3, N. Y.
Atn: Facilities & Resources Branch

Atn: ORDEH-O-TA

Office, Chief of Ordnance
Washington 25, D. C.
Atn: ORDTB

Army Research Office
Duke Station
Durham, North Carolina

Atn: Dr. George Wyman, Box CM
Chemistry Division

Army Materials Research Agency
Watertown Arsenal
Watertown, 72, Mass.

Atn: Mr. A. P. Levitt, Chief
High Temperature Branch

Aberdeen Proving Ground, Maryland
Atn: Ballistic Research
Laboratory ORDBG-BLI

Picatinny Arsenal
Dover, New Jersey
Atn: Library

Diamond Ordnance Fuze Laboratories
Washington 25, D. C.
Atn: ORDTL (012)

U. S. Naval Air Missile Test Center
Point Mugu, California
Atn: Technical Library

U. S. Naval Ordnance Laboratory
White Oak, Silver Spring, Maryland
Atn: Library

U. S. Naval Ordnance Test Station
China Lake, California
Atn: Technical Library Branch

U. S. Naval Propellant Plant
Indian Head, Maryland
Atn: Technical Library

U. S. Naval Weapons Laboratory
Dahlgren, Virginia
Atn: Technical Library

Office of Naval Research
Washington 25, D. C.
Atn: CODE 429, Dr. Ralph Roberts

U. S. Naval Research Laboratory
Washington 20, D. C.
Atn: Chemistry Div. CODE 6130,
R. R. Miller

Bureau of Naval Weapons
Washington 25, D. C.
Atn: RMMP-2

Atn: RMMP-22, Mr. John J. Murrin

Atn: RMMP-3

Atn: RMMP-4

Atn: DLI-3 (2)

Atn: RRRE-6

Special Projects Office
Department of the Navy
Washington 25, D. C.

Aerojet-General Corporation (3)
Sacramento, California
Atn: Technical Information Office

Aerojet-General Corporation
Solid Rocket Plant, Bldg., 0525
Sacramento, Calif.
Atn: James P. Coughlin

Aerojet-General Corporation
Azusa, California
Atn: F. H. West, Chief Librarian

Aerojet-General Corporation
Structural Materials Div.
Azusa, Calif.
Atn: Dr. S. Breiant, Head
Materials Engineering Dept.

Aeronutronic, A. Div. of Philco Corp.
Newport Beach, Calif.
Atn: L. H. Linder, Manager
Technical Information Dept.

Atn: D. L. Hildenbrand

Aerospace Corporation (2)
Los Angeles 45, Calif.
Atn: Library - Documents

Air Force Flight Test Center
Edwards Air Force Base, California
Atn: FTR

Air Force Office of Scientific Research
Department of the Air Force
Washington 25, D. C.
Atn: Dr. Joseph Masi, Chief
Propulsion Div. (SREP)

Air Force Systems Command (2)
Ceramics & Graphite Information Center
Wright-Patterson Air Force Base, Ohio
Atn: MAAM - (Mr. Barry H. Emrich)

Air Force Systems Command
Rocket Research Laboratories
Edwards, California
Atn: DGS

Atn: DGPS, Mr. Curtis C. Selph
Headquarters 6953d Test Group

Air Force Systems Command
Rocket Research Laboratory
Chemical & Materials Branch (DGPC)
Edwards, California 93523
Atn: Mr. Wayne C. Solomon

Air Force Systems Command (2)
Aeronautical Systems Division
Wright-Patterson Air Force Base, Ohio
Atn: Mr. W. G. Ramke, CODE ASRCMC

Atn: ASRCEM-1

Atn: ASRCNC-2

Atn: ASRCMP-2

Atn: ASRCTPT, Mr. Jules J. Wittebort

Air Force Systems Command
United States Air Force
AFSC Scientific & Tech. Liaison Office
New York 3, N. Y.

Air Force Unit Post Office
Space Systems Division
Los Angeles, Calif. 90045
Atn: SSSD

Air Proving Ground Center
Eglin Air Force Base, Florida
Atn: PGAPI

Air Research & Development Command
Headquarters, Wright Air Develop. Div.
Wright-Patterson Air Force Base, Ohio
Atn: WWRCPT-1

Air Research & Development Center
Andrews Air Force Base
Washington 25, D. C.
Atn: RDRAPR

Allied Chemical Corp.
General Chem. Division
Research Laboratory
Morristown, N. J.
Atn: L.J. Wiltrakis, Security Officer

Alpha Research & Development, Inc. (2)
Blue Island, Illinois
Atn: Dr. Robert Patrick

Amcel Propulsion Company
Asheville, North Carolina

American Cyanamid Company
Stamford, Conn.
Atn: Dr. Robert E. Torley
Atn: Dr. A. L. Peiker
Armour Research Foundation of Illinois
Institute of Technology
Chicago 16, Illinois
Atn: Fluid Dynamics & Propulsion
Research Dept. D.

Atn: Dr. Alan Snelson

Astro-Systems, Inc.
Caldwell, New Jersey
Atn: Mr. John S. Gordon

Atlantic Research Corporation
Shirley Highway & Edsall Road
Alexandria, Va.
Atn: Mr. Charles B. Henderson

Atomics International
Canoga Park, Calif.
Atn: S. C. Carniglia, Dept. 733

Avco
Wilmington, Mass.
Atn: Dr. N. L. Schick

Battelle Memorial Institute
Columbus 1, Ohio
Atn: J. F. Lynch, Ceramics Div.

Atn: C. S. Dumont,
Defense Metals Information Center

British Defence Staff (4)
British Embassy
Washington, D. C.
Atn: Scientific Information Center

Borg-Warner Corporation
Ingersoll Kalamazoo Div.
Kalamazoo, Michigan
Atn: Special Projects Dept.

The Carborundum Company
Niagara Falls, N. Y.

Chemical Propulsion Information Agency
Applied Physics Laboratory
Silver Spring, Maryland
Atn: Mr. Gerald Avery

Clevite Corporation
Mechanical Research Division
Cleveland 8, Ohio
Atn: N. C. Beerli

Cornell Aeronautical Laboratories
Buffalo 21, New York
Atn: Mr. J. Beale

DeBell & Richardson, Inc.
Hazardville, Conn.
Atn: Mr. William Eakins

Defense Documentation Center (10)
Alexandria, Va.

Defense Research Member (4)
Canadian Joint Staff (W)
Washington 8, D. C.

The Dow Chemical Company (2)
Midland, Michigan
Atn: Dr. Daniel R. Stull
Thermal Laboratory,
Bldg. 574

Atn: Dr. R. S. Karpiuk
Security Section, Bldg., 1710

E. I. DuPont de Nemours & Co.
Eastern Laboratory
Gibbstown, N. J.
Atn: Mrs. Alice R. Steward

Esso Research & Engineering Co.
Chemicals Research Division
Special Projects Unit
Linden, N. J.
Atn: Mr. D. L. Baeder

Atn: Dr. Walter G. May

Fulmer Research Institute, Ltd.
Stoke Poges, Buckinghamshire, England
Atn: Dr. Philipp Gross

General Electric Company
Flight Propulsion Division
Evendale
Cincinnati, Ohio 45215

General Electric Co.
Nuclear Materials & Propulsion Oper.
Cincinnati, Ohio 45215
Atn: J. W. Stephenson

Hercules Powder Company (2)
Allegany Ballistics Lab.
Cumberland, Maryland
Atn: Library

Hercules Powder Company
Rocky Hill Plant
Rocky Hill, N. J.

Hercules Powder Company (2)
Magna, Utah
Atn: Librarian

Ionics, Inc.
Washington 5, D. C.
Atn: Mr. S. G. McGriff,
Asst. Director of Research

Jet Propulsion Laboratory
Pasadena 3, Calif.
Atn: I. E. Newlan,
Chief Reports Group

Arthur D. Little, Inc.
Cambridge 40, Mass.
Atn: Dr. Alfred Buchler

Atn: Dr. J. B. Berkowitz-Mattuck

Lockheed Propulsion Co. (3)
Redlands, Calif.
Atn: Miss Belle Berlad, Librarian

Manufacturing Laboratories, Inc.
Cambridge 39, Mass.
Atn: Dr. Larry Kaufman

Midwest Research Institute
Kansas City 10, Mo.
Atn: Dr. Thomas A. Milne

Minnesota Mining & Manufacturing Co. (2)
St. Paul 6, Minnesota
Atn: CODE 0013 R&D
Via: H. C. Zeman,
Security Administrator

Minnesota Mining & Manufacturing Co.
Central Research Laboratories
St. Paul 19, Minnesota
Atn: Dr. George Rathmann

National Research Corporation
Cambridge 42, Mass.
Atn: Mr. Ludwig Fasolino

Oak Ridge National Laboratory
Research Materials Information Center
Oak Ridge, Tennessee 37831

Olin Mathieson Chemical Corp. (2)
Research Library 1-K-3
New Haven, Conn.
Atn: Miss Laura M. Kajuti
Mail Control Room

Olin Mathieson Chemical Corp.
Marion, Illinois
Atn: Research Library

Rocketdyne (3)
Canoga Park, Calif.
Atn: Library 596-306

Atn: Mr. Kurt Mueller

Rocketdyne
A Division of No. American Aviation, Inc.
Solid Propulsion Operations
McGregor, Texas
Atn: Library

Rocket Power
Pasadena, Calif.
Atn: Dr. Milton Farber,
Vice President

Shell Development Co.
Emeryville 8, Calif.

Space Technology Lab., Inc.
Redondo Beach, Calif.
Atn: Mr. Robert C. Anderson

Stanford Research Institute
Menlo Park, Calif.
Atn: G. M. Gordon

Thiokol Chemical Corporation
Redstone Division
Huntsville, Alabama
Atn: Technical Director

Thiokol Chemical Corporation
Elkton Division
Elkton, Maryland
Atn: Librarian

Thiokol Chemical Corporation
Reaction Motors Division
Denville, N. J.
Atn: Mr. William Mitchell

Thiokol Chemical Corp. (2)
Wasatch Div.
Brigham City, Utah
Atn: Library Section

Thiokol Chemical Corp.
Rockets Operation Center
Ogden, Utah
Atn: Librarian

United Aircraft Corporation
Research Laboratories
E. Hartford 8, Conn.
Atn: Mr. John D. Rockenfeller

United Technology Center
Sunnyvale, Calif.
Atn: Librarian

Atn: Dr. R. O. MacLaren

University of California
Los Alamos Scientific Lab.
Los Alamos, New Mexico 87544
Atn: Dr. James T. Waber

Dr. Leo Brewer
Department of Chemistry
University of California
Berkeley, California

Dr. S. H. Bauer
Department of Chemistry
Cornell University
Ithaca, New York

Professor R. L. Sproull
Materials Science Center
Cornell University
Thurston Hall
Ithaca, N. Y.

The John Hopkins University (3)
Solid Propellant Information Agency
Applied Physics Laboratory
Silver Spring, Maryland

The John Hopkins University
Applied Physics Laboratory
Silver Spring, Maryland
Atn: Dr. A. Westenberg

Dr. T. E. Phipps
Department of Chemistry
University of Illinois
Champaign-Urbana, Illinois

Dr. Charles J. Marsel
Department of Chemical Engineering
New York University
New York 53, N. Y.

Professor M. E. Fine
Materials Research Center
The Technological Institute
Northwestern University
Evanston, Illinois

Dr. Webster B. Kay
Dept. of Chemical Engineering
Ohio State University
Columbus 10, Ohio

Dr. David White
Department of Chemistry
Ohio State University
Columbus 10, Ohio

Dr. Robert D. Freeman
Department of Chemistry
Oklahoma State University
Stillwater, Oklahoma

Professor J. N. Hobstetter
Laboratory for Res. on Struc. of Matter
University of Pennsylvania
Philadelphia 4, Penna.

Dr. Y. S. Touloukian
Dir., Thermophysical Properties Res. Cen.
Purdue University
West Lafayette, Indiana

Professor J. L. Margrave
Department of Chemistry
Rice Institute
Houston 11, Texas

Dr. K. Keith Innes
Department of Chemistry
Vanderbilt University
Nashville, Tennessee

Professor Paul R. Jones
Dept. of Chemical Engineering
West Virginia University
Morgantown, West Va.

Dr. Paul Bender
Department of Chemistry
University of Wisconsin
Madison, Wisconsin

Dr. Peter McCuen
Vidya Company
Stanford Industrial Park
Palo Alto, Calif.

Westinghouse Electric Co.
Pittsburgh, Pennsylvania
Atn: Dr. Alvin Boltax

Wright Aeronautical Division
Curtiss-Wright Corporation
Woodridge, N. J.

Union Carbide Corporation

Dr. A. L. Bayes

Mr. J. C. Bowman

Dr. J. C. Brantley/
G. H. Clewett/UCN Library

Dr. R. M. Bushong

Mr. M. C. Carosella

Dr. R. A. Charpie

Mr. D. E. Hamby

Dr. A. B. Kinzel

Helen F. Kuhns, Librarian
Union Carbide Stellite Div.

Dr. P. Lafayatis

Dr. R. W. McNamee

Mr. W. Manly

Dr. B. J. Miller

Mr. R. M. Milton

Mr. W. B. Nicholson

Dr. W. J. Spry

Dr. Milton Stern

Mr. W. A. Steiner

Mr. Roy C. Sundeen

Dr. C. E. Sunderlin

Mr. H. F. Wendt/Mr. A. L. Hallowell

Mr. H. L. Willard

Dr. C. E. Winters